SLIDING MODE AND PID BASED TRACKING CONTROL OF MAGNETIC LEVITATION PLANT AND HIL TESTS

A THESIS
SUBMITTED TO THE DEPARTMENT OF ELECTRICAL AND COMPUTER ENGINEERING
AND THE GRADUATE SCHOOL OF NATURAL SCIENCES OF ABDULLAH GUL UNIVERSITY
IN PARTIAL FULFILLMENT OF THE REQUIREMENTS
FOR THE DEGREE
MASTER'S

By
Yakup Eroğlu
January 2016

I certify that I have read this thesis and that in my opinion it is fully adequate, in scope and in quality, as a thesis for the DEGREE MASTER'S.

_____

Supervisor: Assist. Prof. Günyaz Ablay

I certify that I have read this thesis and that in my opinion it is fully adequate, in scope and in quality, as a thesis for the DEGREE MASTER'S.

_____

Jury Member: Assist. Prof. Kutay İçöz

I certify that I have read this thesis and that in my opinion it is fully adequate, in scope and in quality, as a thesis for the DEGREE MASTER'S.

_____

Jury Member: Prof. Recai Kılıç

Approved for the Graduate School of Natural Sciences:

_____

Prof. Dr. İrfan Alan

Director of Graduate School of Natural Sciences

ABSTRACT

SLIDING MODE AND PID BASED TRACKING CONTROL OF MAGNETIC LEVITATION PLANT AND HIL TESTS

Magnetic levitation systems are convenient to provide frictionless, reliable, fast and economical operations in wide-range applications. The effectiveness and applicability of these systems require precise feedback control designs. The position control problem of the magnetic levitation plant can be solved with a cascade control method. In this thesis, sliding mode and PID based cascade controllers are designed to render high position control performance and robustness to the magnetic levitation. Sliding mode control (SMC) based cascade controller is proposed for controlling magnetic levitation. The SMC based controllers for the inner current loop are designed to eliminate the effects of the inductance related uncertainties of the electromagnetic coil of the plant. For the outer position loop, the integral SMC is designed to eliminate disturbances around operating point resulting from the linearization of the mechanical part. Finally, numerical simulation and experimental results for various cascaded controllers are provided and compared in order to validate the efficacy of the approaches.

Yakup Eroğlu
Master's program in Electrical and Computer Engineering Department
Supervisor: Assist. Prof. Günyaz Ablay

January 2016

Keywords: Sliding Mode Control, Cascade Control, Magnetic Levitation, Robust Tracking, Hardware in the Loop Test.

ÖZET

MANYETİK LEVİTASYON SİSTEMİNİN KAYAN KİP VE PID TEMELLİ REFERANS TAKİP KONTROLÜ VE DONANIM İÇEREN BENZETİM TESTLERİ

Manyetik levitasyon sistemleri birçok alanda sürtünmesiz, güvenli, hızlı ve ekonomik işlem sağlamaya yatkındır. Bu sistemlerin etkinliği ve uygulanabilirliği geri beslemeli kontrol tasarımını zorunlu kılar. Manyetik levitasyon sisteminin pozisyon kontrol problemi, kademeli bir kontrol metoduyla çözülebilir. Bu tezde, kayan kip ve PID temelli kademeli kontrolörler, manyetik levitasyon sistemine yüksek pozisyon kontrol performansı ve dayanıklılığı mümkün kılmak için tasarlandı. Kayan kip temelli kademeli kontrolör manyetik levitasyonu kontrol etmek için önerildi. Ek olarak, iç akım döngüsünün kayan kip temelli kontrolörleri, sistemin elektromanyetik bobinin indüktans ilişkili belirsizliklerin etkilerini elemek için tasarlandı. Dış pozisyon döngüsü için kayan kip temelli kontrolörler, mekanik bölümün doğrusallaştırılmasından kaynaklı denge noktasındaki bozucuları elemek için tasarlandı. Sonuç olarak, bütün kademeli tasarlanmış kontrolörlerin nümerik simülasyon ve deneysel sonuçları, metodun etkinliğini göstermek için gösterildi ve kıyaslandı.

Yakup Eroğlu
Elektrik ve Bilgisayar Mühendisliği Ana Bilim Dalı, Yüksek Lisans Programı
Tez Yöneticisi: Yrd. Doç. Dr. Günyaz Ablay
Ocak 2016

Anahtar kelimeler: Kayan Kipli Kontrol, Kademeli Kontrol, Manyetik Levitasyon, Dayanıklı Referans Takibi, Donanım İçeren Test.

Acknowledgements

I would like to express my very great appreciation to Assistant Professor Günyaz ABLAY, my supervisor, for his invaluable and constructive suggestions in addition to his guidance and enthusiastic encouragement during my time at Abdullah Gül University.

I would also like to thank the Scientific and Technological Research Council of Turkey (TÜBİTAK) for supporting my studies during my Master of Science education under project number 113E329.

Biography

Yakup Eroğlu was born in 1987, Kayseri, Turkey. He obtained his BSc in 2014 from Department of Electronics-Communication Engineering, İzmir Institute of Technology. His major undergraduate studies were focused on measurement of heart rate with a reflective sensor. He is currently an MSc student in Electrical and Computer Engineering at Abdullah Gül University. He currently works on a TUBITAK project related to sliding mode control development for processes and its practical implementations.

Publications:

Y. Eroğlu and G. Ablay, "Cascade control of magnetic levitation with sliding modes," *International Conference on Control, Mechatronics and Automation (ICCMA 2015)*, Barcelona, Spain, 2015.

Y. Eroğlu and G. Ablay, "PI-V plus sliding mode based cascade control of magnetic levitation," *International Conference on Electrical and Electronics Engineering (ELECO 2015)*, pp. 785-789, Bursa, Turkey, 2015.

G. Ablay ve Y. Eroğlu, "Variable structure controllers for processes," *Turkish Automatic Control Conference (TOK 2015)*, Denizli, pp. 268-273 , 2015 (in Turkish).

G. Ablay and Yakup Eroğlu, "Integral sliding mode control of DC servo-driven conveyor system," *Applied Mechanics and Materials*, vol. 799-800, pp. 1177-1182, 2015.

G. Ablay and Yakup Eroğlu, "Integral sliding mode control of DC servo-driven conveyor system," *International Conference on Automatic Control (ICOAC 2015)*, Ankara, Turkey, 2015.

Table of Contents

1. **INTRODUCTION 1**

1.1 PID CONTROLLER DESIGN 4
1.2 SLIDING MODE CONTROLLER DESIGN 5

2. **MAGNETIC LEVITATON AND ITS MODELLING 8**

2.1 MODELING OF THE ELECTRICAL PART 11
2.1.1 Electrical Model for Constant Coil Inductance 11
2.1.2 Electrical Model for Position Dependent Coil Inductance 12
2.2 MODELING OF THE MECHANICAL PART 13
2.3 LINERIZATION OF NONLINEAR MECHANICAL PART 14

3. **CONTROLLER DESIGN 16**

3.1 DESIGN OF THE INNER CONTROLLERS 18
3.1.1 PI Controller 19
3.1.2 High-Gain Sliding Mode Controller 20
3.1.3 Process Sliding Mode Controller 21
3.1.4 Sliding Mode Control Designs under Varying Coil Inductance 22
3.2 DESIGN OF THE OUTER CONTROLLERS 26
3.2.1 PI plus Velocity Controller 27
3.2.2 Integral Sliding Mode Controller 30

4. **RESULTS 34**

4.1 PI-V PLUS PI CASCADE CONTROL 36
4.1.1 Numerical Simulations 36
4.1.2 Experimental Results 39
4.2 PI-V PLUS PROCESS SMC CASCADE CONTROL 42
4.2.1 Numerical Simulations 43
4.2.2 Experimental Results 45
4.3 INTEGRAL SMC PLUS PROCESS SMC CASCADE CONTROL 49
4.3.1 Numerical Simulations 50
4.3.2 Experimental Results 52
4.4 INTEGRAL SMC PLUS EQUIVALENT SMC CASCADE CONTROL WITH VARYING INDUCTANCE 55
4.4.1 Numerical Simulations 55
4.4.2 Experimental Results 58
4.5 COMPARISON OF CASCADE CONTROLLERS 62
4.5.1 Numerical Simulations 62
4.5.2 Experimental Results 64

5. **CONCLUSIONS 66**

BIBLIOGRAPHY 67

APPENDIX A: SIMULINK PROGRAMS 70

APPENDIX B: TAYLOR SERIES APPROXIMATION 75

List of Figures

Figure 1.1 Maglev train. 2
Figure 1.2 Magnetic bearing and induction heater 2
Figure 1.1.1 Block scheme of PID controller. 4
Figure 1.2.1 Block scheme of SMC controller 6
Figure 1.2.2 The state-space of error dynamics around sliding surface 6
Figure 2.1 Schematic diagram of a single-axis magnetic levitation system. 9
Figure 2.2 Dynamical modeling of the magnetic levitation plant.. 10
Figure 3.1 A cascade control block diagram of the magnetic levitation system 16
Figure 3.1.1 Block diagram for the inner current loop 18
Figure 3.2.1 Block diagram for the outer position loop 27
Figure 4.1.1.1 Ball position trajectory for PI-V plus PI 37
Figure 4.1.1.2 Coil current response for PI-V plus PI 37
Figure 4.1.1.3 Coil voltage response for PI-V plus PI 38
Figure 4.1.1.4 Position tracking error for PI-V plus PI 38
Figure 4.1.1.5 Current tracking error for PI-V plus PI 39
Figure 4.1.2.1 Experimental ball position trajectory for PI-V plus PI 40
Figure 4.1.2.2 Experimental coil current response for PI-V plus PI 40
Figure 4.1.2.3 Experimental coil voltage response for PI-V plus PI 41
Figure 4.1.2.4 Experimental position tracking error for PI-V plus PI 41
Figure 4.1.2.5 Experimental current tracking error for PI-V plus PI 42
Figure 4.2.1.1 Ball position trajectory for PI-V plus PSMC 43
Figure 4.2.1.2 Coil current response for PI-V plus PSMC 44
Figure 4.2.1.3 Coil voltage response for PI-V plus PSMC 44
Figure 4.2.1.4 Position tracking error for PI-V plus PSMC 44
Figure 4.2.1.5 Current tracking error for PI-V plus PSMC 45
Figure 4.2.2.1 Experimental ball position trajectory for PI-V plus PSMC 46
Figure 4.2.2.2 Experimental coil current response for PI-V plus PSMC 46
Figure 4.2.2.3 Experimental coil voltage response for PI-V plus PSMC 47
Figure 4.2.2.4 Experimental position tracking error for PI-V plus PSMC 47
Figure 4.2.2.5 Experimental current tracking error for PI-V plus PSMC 47
Figure 4.2.2.6 Experimental ball position trajectory for a sinusoidal reference of PI-V plus PSMC 48
Figure 4.2.2.7 Experimental coil current response for a sinusoidal reference of PI-V plus PSMC 48
Figure 4.2.2.8 Experimental coil voltage response for a sinusoidal reference of PI-V plus PSMC 48
Figure 4.2.2.9 Experimental position tracking error for a sinusoidal reference of PI-V plus PSMC 49

Figure 4.2.2.10 Experimental current tracking error for a sinusoidal reference of PI-V plus PSMC 49
Figure 4.3.1.1 Ball position trajectory for ISMC plus PSMC 50
Figure 4.3.1.2 Coil current response for ISMC plus PSMC 51
Figure 4.3.1.3 Position tracking error for ISMC plus PSMC 51
Figure 4.3.1.4 Current tracking error for ISMC plus PSMC 51
Figure 4.3.1.5 Sliding surface of outer ISMC for ISMC plus PSMC 52
Figure 4.3.2.1 Experimental ball position trajectory for ISMC plus PSMC 53
Figure 4.3.2.2 Experimental coil current response for ISMC plus PSMC 53
Figure 4.3.2.3 Experimental position tracking error for ISMC plus PSMC 53
Figure 4.3.2.4 Experimental current tracking error for ISMC plus PSMC 54
Figure 4.3.2.5 Experimental sliding surface of outer ISMC for ISMC plus PSMC 54
Figure 4.3.2.6 Experimental ball position trajectory in the steady-state for ISMC plus PSMC 54
Figure 4.3.2.7 Experimental position tracking error in the steady-state for ISMC plus PSMC 55
Figure 4.4.1.1 Ball position trajectory for ISMC plus eSMC with varying inductance 56
Figure 4.4.1.2 Coil current response for ISMC plus eSMC with varying inductance 56
Figure 4.4.1.3 Position tracking error for ISMC plus eSMC with varying inductance 57
Figure 4.4.1.4 Coil current tracking error for ISMC plus eSMC with varying inductance 57
Figure 4.4.1.5 Sliding surface of outer ISMC for ISMC plus eSMC with varying inductance 58
Figure 4.4.2.1 Experimental ball position trajectory for ISMC plus eSMC with varying inductance 59
Figure 4.4.2.2 Experimental coil current response for ISMC plus eSMC with varying inductance 60
Figure 4.4.2.3 Experimental position tracking error for ISMC plus eSMC with varying inductance 60
Figure 4.4.2.4 Experimental coil current tracking error for ISMC plus eSMC with varying inductance 61
Figure 4.4.2.5 Experimental sliding surface of outer ISMC for ISMC plus eSMC with varying inductance 61

List of Tables

Table 2.1 Plant model parameters 10
Table 4.5.1.1 Position tracking performance of numerical studies for all cascaded controllers 63
Table 4.5.2.1 Position tracking performance of experimental studies for all cascaded controllers 65

This document is dedicated to my family.

Chapter 1

Introduction

Magnetic levitation technology is used to levitate an object (e.g., made of nickel, cobalt, iron, etc.) with no support other than magnetic field force. It makes frictionless and contactless movements possible. So, magnetic levitation technology is very important for many industrial systems including maglev trains, electromagnetic bearings, electromagnetic cranes, levitation of wind tunnel models, vibration isolation of sensitive machinery, levitation of molten metal in induction furnaces, rocket-guiding projects, levitation of metal slabs during manufacture and high-precision positioning of wafers in photolithography [1–8]. I would like to explain some of them. Firstly, the maglev train shown in Fig. 1.1 has high-speed and the energy efficiency because they do not have friction problem excluding air. Secondly, magnetic bearing shown in Fig. 1.2 is a bearing that supports a load using magnetic levitation. Magnetic bearings reinforce movable parts of the system by eliminating direct contact between materials. Such support includes levitation of a rotating shaft and almost frictionless movement and they do not have mechanical wear. In addition, induction heater shown in Fig. 1.2b is used to smelt or heat metal by levitating the metal. Induction heating is critical in most of the manufacturing industry because of its attractive advantages such as good speed, precision and control.

Figure 1.1 Maglev train.

Figure 1.2 Magnetic bearing and induction heater.

Magnetic levitation technology is able to serve reliable and high-speed operations with the use of feedback controllers. On the other hand, it is difficult to provide high control performance with standard controllers for the magnetic levitation systems because of some control problems. First of all, they have open-loop unstable mechanical part. Secondly, they include highly nonlinear dynamics. Finally, the coil inductance value is assumed as a constant but it depends on the steel position to be controlled, so there exists parameter uncertainty due to inductance of the electromagnetic coil. Thus, a robust

controller is needed for controlling of the magnetic levitation system. In this thesis, I will use a sliding mode controller (SMC) to increase the system performance and to eliminate disturbances due to its robustness feature.

Recently, many works have been reported for controlling magnetic levitation in the literature. The designed control techniques include feedback linearization based controllers (including input-output and input-state linearization techniques) [4], [6], [9–11], observer-based control [5], linear state feedback control design [6,12], the gain scheduling approach [13], neural network techniques [14], sliding mode controllers [8,15,16], backstepping control [17], model predictive control [18] and PID controllers [19]. In short, many known linear and nonlinear control methods were designed for magnetic levitation systems. In the linear controller designs, the approximate linear model found by perturbing the system dynamics about a desired operating point is used, and thus, the controller are usually valid only around the operating point. The performance of the linear controllers can be improved with some kind of gain scheduling procedure to change operating points, but the stability may not be guaranteed. So, the nonlinear controllers seem more attractive as the system consists highly nonlinearity. However, many nonlinear control designs need exact knowledge about the plant nonlinearities to ensure a good performance. The modeling and parameter uncertainties in the magnetic levitation plant model makes practical implementations of the nonlinear controllers difficult.

In this thesis, a practical cascade control approach is proposed. The cascade control allows us to design a more stable and robust inner current controller to deal with the effects of plant disturbance and uncertainty. Because the magnetic levitation plant consists of the mechanical and electrical parts, the cascade controller can give a good performance.

The cascade controller includes an inner part and an outer part control loop. In nature, the electrical part is much faster than the mechanical part. So, our inner loop controller should be faster than our loop controller. Thus, in this thesis, for the electrical part which is much faster than the mechanical part, the PI (proportional plus integral) controller and several SMC controllers are

designed to give fast response for the inner loop. The SMC has ability to high performance current controller and to render robustness in the presence of inductance uncertainties due to the coil inductance. For the mechanical part of the system, a PI plus velocity (V), SMC and integral SMC controllers are designed for tracking control of the position of the magnetic levitation plant. The SMC and integral SMC (ISMC) are able to eliminate disturbances around the operating point. The position tracking performances of the cascaded controllers are demonstrated with numerical simulations and experimental results.

This thesis is organized as follows: Section 2 provides a background on magnetic levitation system. Controller design strategies are given in Section 3. Numerical simulations, experimental results and comparisons are given in Section 4. Conclusions of the thesis are provided in Section 5.

Before Section 2, I would like to mention about a general PID and a general SMC design procedure since the cascade controllers to be designed in this thesis are based on PID and SMC controllers.

1.1 PID Controller Design

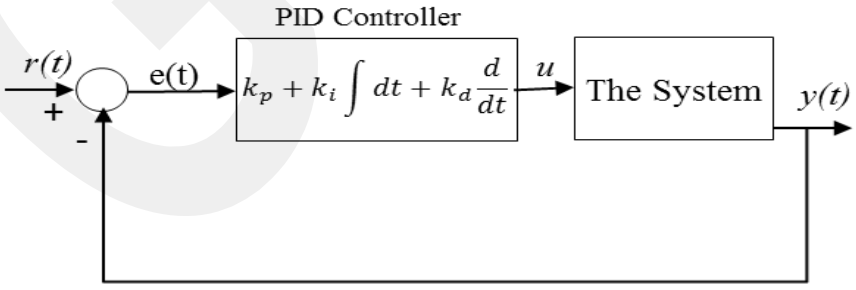

Figure 1.1.1 Block scheme of PID controller.

PID controller is designed as shown in Fig. 1.1.1. Here, r is the reference input, e is the tracking error we want to keep it around zero, u is the control input, designed PID controller which consists of proportional, integral and

derivative gains, i.e., the control gains, k_p, k_i and k_d. PID controller is described by

$$u(t) = k_p e(t) + k_i \int e(t)dt + k_d \frac{de(t)}{dt} \quad \textbf{(1.1.1)}$$

where $e(t) = r(t) - y(t)$. The system output with Laplace transform of Equation (1.1.1) can be written as

$$Y(s) = G(s)\left[k_p + \frac{k_i}{s} + k_d s \right](R(s) - Y(s)) \quad \textbf{(1.1.2)}$$

where $G(s)$ is the open loop transfer function of the system, and $E(s) = R(s) - Y(s)$ is the tracking error in the Laplace domain. Thus, the closed loop transfer function can be obtained from Equation (1.1.2) as follows

$$\frac{Y(s)}{R(s)} = \frac{(k_d s^2 + k_p s + k_i)G(s)}{(k_d s^2 + k_p s + k_i)G(s) + s} \quad \textbf{(1.1.3)}$$

The roots of the denominator of the closed loop transfer function of the system should be negative for the stability. The gains, k_p, k_i and k_d must be selected appropriately to provide the stability and a good performance. There are some methods to find the gains, such as pole placement method and empirical tuning methods (e.g. Ziegler-Nichols method). In this thesis, I use the pole placement method to find the gains for providing stability. According to this method, the denominator of the closed loop transfer function is equated to the characteristic function which is obtained from the desired system requirements. Thus, the gain parameters of the PID controller, k_p, k_i and k_d are obtained for providing the desired stability and performances.

1.2 Sliding Mode Controller Design

A sliding mode controller is designed as shown in Fig. 1.2.1. Here, r is the reference input, e is the tracking error and u is the control input. The sliding

surface (s) we want to keep it around zero is designed in the SMC design. The sliding surface, s, can be expressed as follows [20]

$$s = e\left[\frac{d}{dt} + \lambda\right]^{n-1} \qquad \textbf{(1.2.1)}$$

where $e = r(t) - y(t)$ and λ should be bigger than zero ($\lambda > 0$), and n is the degree of the system (the system's order).

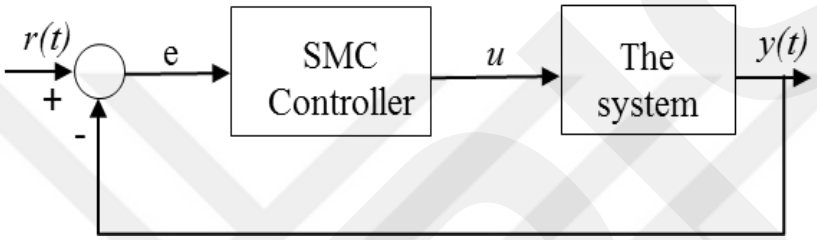

Figure 1.2.1 Block scheme of SMC controller.

For $n = 2$, state-space diagram of error dynamics around sliding surface is shown in Fig. 1.2.2. Here, sliding mode controller brings any tracking error (e) trajectory to the sliding surface and keeps it on that surface. If the SMC keeps the system trajectory on the sliding surface, then this mode is called as sliding mode, and during sliding mode we have $s = \dot{s} = 0$.

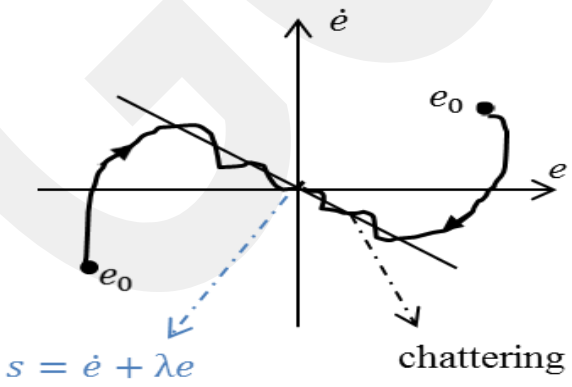

Figure 1.2.2 The state-space diagram of error dynamics around sliding surface.

During the sliding mode, the equivalent (average) control input, u_{eq}, can be found from $\dot{s} = 0$, and it is the necessary control action to keep the system on the sliding mode.

The control input, u, usually consists of the combination of equivalent control and a discontinuous controller as follows

$$u = u_{eq} + u_0 \operatorname{sgn}(s) \tag{1.2.2}$$

where

$$\operatorname{sgn}(s) = \begin{cases} 1 & if \quad s > 0 \\ -1 & if \quad s < 0 \end{cases} \tag{1.2.3}$$

By achieving the Lyapunov based reachability (or stability) condition ($s\dot{s} < 0$), which is obtained from the Lyapunov stability theorem [20,21], the range of control gain parameter, u_0, can be found to ensure stability. The most appropriate gain value can be obtained via simulation. It should be noted that in practical implementations of the SMC, the saturation function $sat(s)$, can be used instead of $sgn(s)$ to eliminate chattering on the system output. Chattering is defined as small oscillations in the system trajectory. Chattering is an unwanted phenomenon because it causes power loss in electrical parts, wearing out in mechanical parts, and decreasing the system's life span.

In the following Chapters, the SMC design summarized above will be studied in detail for the magnetic levitation system.

Chapter 2

Magnetic Levitation and its Modeling

Magnetic levitation technology does not establish a contact with the earth and it does not have any friction problem excluding air friction. Therefore, it has been used in many industrial systems including the high-speed maglev trains, electromagnetic bearings, electromagnetic cranes, levitation of wind tunnel models, vibration isolation of sensitive machinery, levitation of molten metal in induction furnaces, rocket-guiding projects, levitation of metal slabs during manufacture and high-precision positioning of wafers in photolithography [1–8]. In my thesis study, I examine a basic form of the magnetic levitation system which includes controlling of the steel ball, through vertical x-axis. Both numerical simulations and HIL (Hardware in the Loop) tests or experimental studies will be performed. I intend to continue my study on magnetic levitation based applications including maglev trains, electromagnetic robots, etc, in the future.

The magnetic levitation system is used to levitate a steel ball in air due to the electromagnetic force created by an electromagnet. The system is made of an electromagnet, a steel ball and a position measurement sensor. A graphical representation of the magnetic levitation system for single-axis control used in the experimental studies is shown in Fig. 2.1.

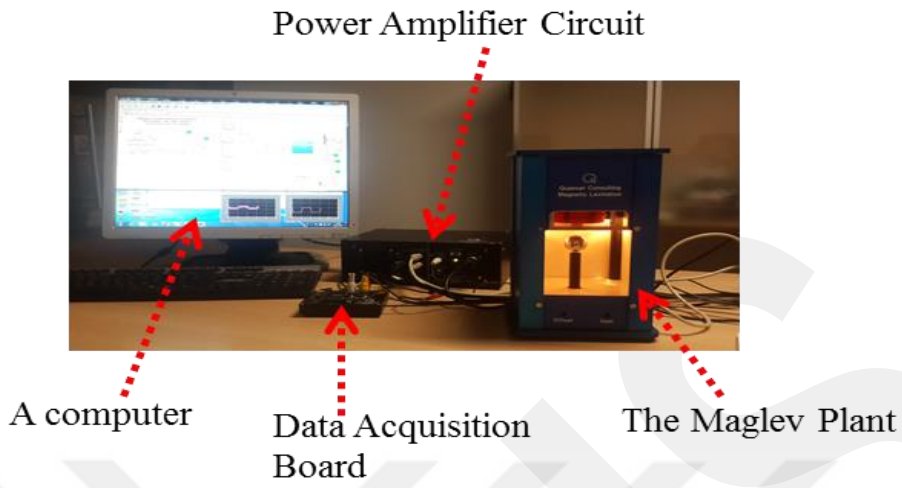

Figure 2.1 Schematic diagram of a single-axis magnetic levitation system.

First of all, a computer is used to control the steel ball. MATLAB/Simulink can be used to design controllers for numerical and experimental results. Secondly, the data acquisition device is used to collect data from sensors and convert digital control data to analog form to drive power amplifier during the operation of the magnetic levitation plant. Another part, the power amplifier is used to amplify the signal to make it capable of proceeding in magnetic levitation plant. Final part is the magnetic levitation plant, which is covered in a rectangular enclosure containing three separate sections. The upper section has an electromagnet, made of a solenoid coil with a steel core. The middle section includes a chamber where the ball suspension takes place. One of the electromagnet poles faces the top of a black post upon which a one inch steel ball rests. A photo sensitive sensor embedded in the post measures the ball elevation from the post. The last section of the system houses the signal conditioning circuitry needed for light intensity position sensor. The ball is only controlled through vertical x-axis in Fig. 2.2. The attraction force is controlled by the computer controlled electromagnet mounted directly above the levitation ball. The photo detector consists of an NPN silicon photodarlington. The electromagnet is composed of a tightly wound solenoid coil made of 2450 turns of 20 AWG magnet wire. Electromagnet coil input supply is ±24V with a maximum 3A coil current. The data acquisition board is a successive

approximation type, 12-bit analog and digital conversion board capable of 4 kHz sampling. In this work, the controllers are implemented at a sampling rate of 1 kHz. The other plant parameters used in numerical and experimental studies are given in Table 2.1.

Symbol	Description	Value
L_c	Coil inductance	412.5mH
R_c	Coil resistance	10Ω
R_s	Current sense resistance	1Ω
K_m	Electromagnet force constant	6.53×10^{-5} Nm^2/A^2
M_b	Steel ball mass	0.068kg
K_B	Position sensor sensitivity	2.83×10^{-3}m/V
N_c	Number of turns in coil wire	2450
μ_0	Magnetic permeability constant	$4\pi \times 10^{-7}$H/m

Table 2.1 Plant model parameters

The magnetic levitation system consists of two main systems, namely mechanical and electrical subsystems, as seen in Fig. 2.2. The electromagnet is modeled with the R_c-L_c circuit while the mechanical part is expressed in terms of acting forces.

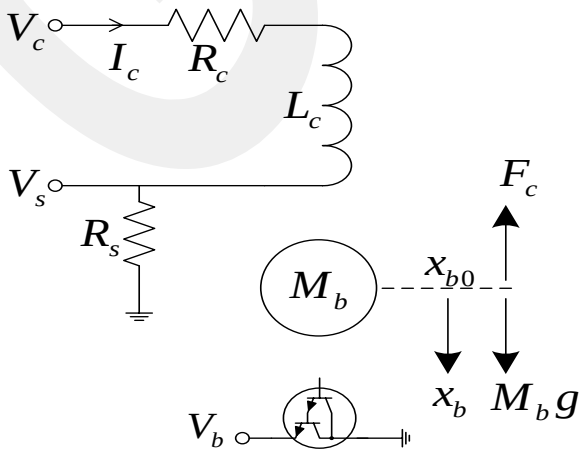

Figure 2.2 Dynamical modeling of the magnetic levitation plant.

The ball position of the mechanical part of the system is controlled via the coil current, I_c, whereas the coil current of the electrical part of the system is regulated with the applied voltage. Therefore, the voltage applied to the electromagnet indirectly controls the ball position. In the following subsections, we can obtain the both mathematical model of the system by using Fig. 2.2.

2.1 Modeling of the Electrical Part

The coil inductance value is dependent on the ball position, x_b, and we can assume it as a constant around the operation point (x_{b0}, I_{c0}), but there exists a parameter uncertainty on the coil inductance with or without this assumption. Thus, we need to design a robust controller to eliminate the effects of this parameter uncertainty.

By applying Kirchhoff's voltage law to the electromagnet modeled by the RL circuit as seen Fig. 2.2, we can get the model of the electrical part directly. On the other hand, the electrical model can be expressed in two different ways, i.e., one model for the constant coil inductance assumption and the other model for the ball-position dependent inductance.

2.1.1 Electrical Model for Constant Coil Inductance

By assuming that the coil inductance is constant around the operation point $(x_{b0},\ I_{c0})$ and applying Kirchhoff's voltage law to the electromagnet (RL circuit in Fig. 2.2.), the electrical model of the magnetic levitation plant can be written as

$$\frac{dI_c}{dt} = -\frac{R_c + R_s}{L_c} I_c + \frac{1}{L_c} V_c \qquad \textbf{(2.1.1.1)}$$

where I_c is the coil current, L_c is the coil inductance(in Henry), R_c is the coil resistance(in Ω), R_s is the current sense resistance(in Ω) and V_c is the supply voltage(in V). The transfer function of the electrical circuit can be obtained by Laplace transform to Equation (2.1.1.1)

$$G_c(s) = \frac{I_c(s)}{V_c(s)} = \frac{K_c}{\tau_c s + 1} \qquad \textbf{(2.1.1.2)}$$

where $K_c = \frac{1}{R_c + R_s}$ is the dc gain, and $\tau_c = \frac{L_c}{R_c + R_s}$ is the time constant of the electrical subsystem. Electrical part is linear and open loop system is stable due to location of pole on the left half of the s-plane. In nature, the electrical subsystem is much faster than the mechanical subsystem. This is good feature for the design of cascade control system (see Chapter 3). All system parameters are given in Table 2.1.

2.1.2 Electrical Model for Position Dependent Coil Inductance

The coil inductance is dependent on the ball position, x_b, and is given by [6,22]

$$L_c(x_b) = L_1 + \frac{K_m}{x_b} \qquad \textbf{(2.1.2.1)}$$

Thus, the inductance L_c has its largest value when the ball is next to the coil, but decreases to a constant L_1 as x_b goes to infinity. L_1 is the constant value, 412.5mH. If the coil inductance is assumed as a constant, this causes parameter uncertainty, and thus we need a robust controller. Otherwise, we can use the dependent function to the ball position, x_b, in Equation (2.1.2.1). Hence, by applying Kirchhoff's voltage law to the electromagnet (RL circuit in Fig. 2.2.), the electrical model of the magnetic levitation plant can be written as

$$(R_c + R_s)I_c + \frac{d\left[L_c(x_b)I_c\right]}{dt} = V_c \qquad \textbf{(2.1.2.2)}$$

where chain rule is

$$\frac{d\left[L_c(x_b)I_c\right]}{dt} = \frac{d\left[L_c(x_b)\right]}{dt} I_c + L_c(x_b)\frac{dI_c}{dt} \qquad \textbf{(2.1.2.3)}$$

By substituting Equation (2.1.2.1) into Equation (2.1.2.2) and applying chain rule, we get the open loop stable and nonlinear electrical model as

$$\frac{dI_c}{dt} = -\frac{R_c + R_s}{L_c} I_c + \frac{K_m}{L_c}\frac{I_c \dot{x}_b}{x_b^2} + \frac{1}{L_c} V_c \qquad \textbf{(2.1.2.4)}$$

where I_c is the coil current, L_c is the dependent coil inductance (in H), R_c is the coil resistance (in Ω), R_s is the current sense resistance (in Ω) and V_c is the supply voltage (in V). The ball position should satisfy $x_b \neq 0$ for validity of the electrical model (i.e., ball never touches the electromagnet during operations).

2.2 Modeling of the Mechanical Part

Using the notation and conventions given in Fig. 2.2, the mechanical model of the magnetic levitation plant can be obtained. Attractive force generated by the electromagnet is given by [23]

$$F_c = \frac{K_m}{2}\left(\frac{I_c}{x_b}\right)^2 \qquad \textbf{(2.2.1)}$$

where K_m is the electromagnet force constant (in Nm^2/A^2) and I_c is the coil current (in A). F_c is nonlinear function, we can linearize around equilibrium point (x_{b0}, I_{c0}). By applying Newton's second law of motion to the ball in Fig. 2.2, the force balance equation of the ball is given with the following second-order model:

$$M_b \ddot{x}_b = M_b g - F_c \qquad \textbf{(2.2.2)}$$

where x_b is the air gap (in m), m is the mass of the ball (in kg), g is the gravitational constant (in m/s^2) and F_c is the force generated by the electromagnet (in N). At equilibrium point, all the time derivative terms are set to zero:

$$-\frac{1}{2}\frac{K_m I_c^2}{M_b x_b^2} + g = 0 \qquad \textbf{(2.2.3)}$$

From Equation (2.2.3), the coil current at equilibrium position, I_{c0}, can be expressed as a function of x_{b0} and K_m, namely,

$$I_{c0} = \sqrt{\frac{2M_b g}{K_m}} x_{b0} \qquad \textbf{(2.2.4)}$$

The operating coil current, I_{c0}, for the electromagnet ball pair can be found at the system's static equilibrium. The static equilibrium at a nominal operating point (x_{b0}, I_{c0}) is characterized by the ball being suspended in air at a stationary point x_{b0} due to a constant attractive force created by I_{c0}.

2.3 Linearization of Nonlinear Mechanical Part

In order to analyze the magnetic levitation, the system can be linearized around equilibrium point (x_{b0}, I_{c0}) at which the system will converge to it as time tends to infinity. Applying Taylor series approximation about equilibrium point (x_{b0}, I_{c0}) to Equation (2.2.2), we get

$$\frac{d^2 x_b}{dt^2} = -\frac{1}{2}\frac{K_m I_{c0}^2}{M_b x_{b0}^2} + g + \frac{K_m I_{c0}^2 x_b}{M_b x_{b0}^3} - \frac{K_m I_{c0} I_c}{M_b x_{b0}^2} \qquad \textbf{(2.3.1)}$$

Substituting Equation (2.2.4) into Equation (2.3.1), we get

$$\frac{d^2 x_b}{dt^2} = \frac{2g x_b}{x_{b0}} - \frac{2g I_c}{I_{c0}} \qquad \textbf{(2.3.2)}$$

Thus, applying Laplace transform in Equation (2.3.2), the transfer function of linearized system around the operation point is obtained as

$$G_b(s) = \frac{X_b(s)}{I_c(s)} = -\frac{K_b w_b^2}{s^2 - w_b^2} \qquad \textbf{(2.3.3)}$$

where $K_b = x_{b0}/I_{c0}$ and $w_b = \sqrt{2g/x_{b0}}$. In this thesis, it is assumed that the operating point of the system is about x_{b0}=6mm and then I_{c0} can be found as $I_{c0} 0.86A$. The open-loop transfer function of the second-order system is type

zero system as it does not contain any pole at the origin. The two open loop poles of the system are located at $s = \pm w_b$ which indicates that the open loop system is unstable due to location of poles on the right-half of the s-plane. Thus, a feedback controller must be designed to stabilize the system.

Chapter 3

Controller Design

Recently, many works have been reported for controlling magnetic levitation in the literature. The designed control techniques include feedback linearization based controllers (including input-output and input-state linearization techniques) [4], [6], [9–11], linear state feedback control design [6,12] the gain scheduling approach [13], observer-based control [5], neural network techniques [14], sliding mode controllers [8,15,16], back-stepping control [17], model predictive control [18] and PID controllers [19]. All these methods have their own advantages and disadvantages. On the other hand, a cascade control system can often perform better than a traditional controller, and advanced control method designs can be included in the cascade control system to perform better than the above designs. Therefore, I focus on a cascade control for the magnetic levitation system for providing stability, robustness and a highly satisfactory position tracking performance. The cascade control approach is proposed to indirectly control ball position for magnetic levitation system as shown in Fig. 3.1 where x_{ref} is reference position, e is the position error, I_r is the controlled reference current due to outer controller, s is the current error. The coil current, I_c, and the ball position, x_b, are to be controlled with the inner and outer controllers, respectively.

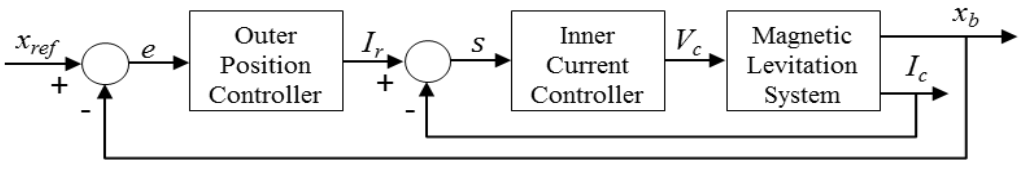

Figure 3.1 A cascade control block diagram of the magnetic levitation system.

The cascade control design consists of an inner controller and an outer controller. An outer loop controller generates a control effort that serves as the setpoint for an inner loop controller. That controller in turn uses the actuator to apply its control effort directly to the inner loop process. The inner loop process then generates a secondary process variable that serves as the control effort for the primary (outer loop) process. The inner loop functions like a traditional feedback control system with a setpoint, a process variable, and a controller acting on a process by means of an actuator. The outer loop does the same except that it uses the entire inner loop as its actuator. Naturally, a cascade control system can't solve every feedback control problem, but it can prove advantageous if under the right circumstances: (a) The inner loop is faster than the outer loop. The secondary process must react to the inner controller's efforts at least three or four times faster than the primary process reacts to the outer controller. This allows the inner controller enough time to compensate for inner loop disturbances before they can affect the primary process. (b) The inner loop has influence over the outer loop. The actions of the inner loop controller must affect the primary process variable in a predictable and repeatable way or else the outer loop controller will have no mechanism for influencing its own process. (c) The inner loop disturbances are less severe than the outer loop disturbances. Otherwise, the inner controller will be constantly correcting for disturbances to the inner loop process and unable to apply consistent corrective efforts to the primary process.

Since the magnetic levitation system fits well to the cascade control design requirements, in this thesis, the inner controller is designed to control the coil current, I_c, for the electrical part of magnetic levitation system and the outer controller is designed to control the ball position, x_b, for the mechanical part of magnetic levitation system. Thus, the ball position of the mechanical part the system is stabilized with the coil current, while the coil current of the electrical part of the system is controlled with the applied voltage. This means that the ball position is indirectly controlled by the electrical voltage source. Firstly, I want to

mention about the design of inner controllers to control the coil current, I_c. Next, I will explain the design of outer controllers to control the ball position, x_b.

3.1 Design of the Inner Controllers

The inner controller is designed to control the coil current, I_c, for the electrical part of magnetic levitation system. Thus, the coil voltage is varied to control the coil current in an electrical system. In the cascade control design, the inner controller should give more fast response than the outer controller since the inner part firstly should control the coil current, I_c, and should not be late from the outer controller for the response. In this context, PI (Proportional and Integral), sliding mode based controllers are designed to control the coil current. In this thesis, PI, high-gain sliding mode, process sliding mode and sliding mode with time-varying inductance, which depends on the ball position, based controllers are designed to control the coil current for the electrical part of magnetic levitation system as shown in Fig. 3.1.1. A voltage limiter is used to limit the coil voltage value $(\pm 24V)$ in the inner controller due to the specification of magnetic levitation system.

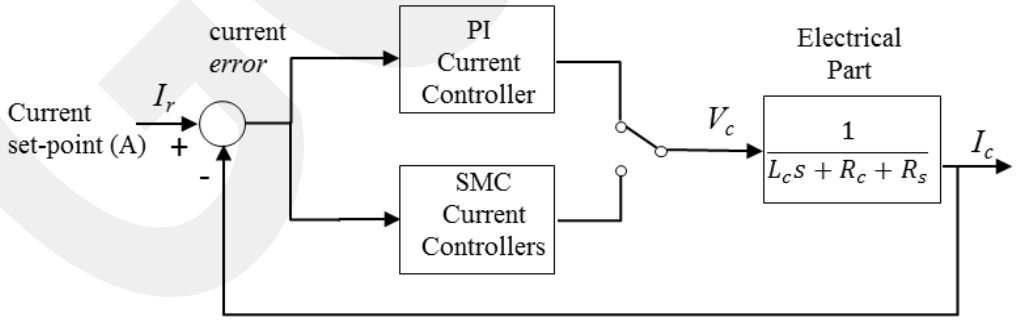

Figure 3.1.1 Block diagram of the inner current loop.

It is difficult to provide high control performance with standard controllers for the magnetic levitation systems because of their open-loop unstable mechanical part and highly nonlinear dynamics, and existence of parameter uncertainties due to the assumption of the coil inductance value as a

constant. Since the SMC has ability to render robustness in the presence of inductance uncertainties, a high-gain sliding mode controller (SMC) and process SMC (PSMC) are designed for ensuring high performance and robustness to current controller. The PSMC is especially designed to deal with chattering problem possibility. Furthermore, the equivalent controller is added to both SMCs to remove the effects of the time-varying coil inductance in an effective way.

3.1.1 PI Controller

Prior to control the ball position, the current flowing through the electromagnet needs to be controlled. Proportional plus integral (PI) controller is designed to control the coil current, I_c, for the electrical part of magnetic levitation system.

The desired performance requirements for the coil current control are as follows

1) Percent overshoot (PO) ≤ 1.5%.
2) Peak time ($t_{p,c}$) ≤ 0.05s.

The amount of overshoot depends just on the damping ratio parameter, ζ, and it is described by

$$PO = 100e^{\left(-\frac{\pi\zeta}{\sqrt{1-\zeta^2}}\right)} \qquad \textbf{(3.1.1.1)}$$

The peak time depends on both the damping ratio, ζ and natural frequency, $\omega_{n,c}$ of the system and it can be derived as

$$t_{p,c} = \frac{\pi}{w_{n,c}\sqrt{1-\zeta^2}} \qquad \textbf{(3.1.1.2)}$$

Thus, the damping ratio and natural frequency can be found as 0.802 and 104.9 rad/s, respectively, from Equation (3.1.1.1) and (3.1.1.2) by using the desired performance requirements. On the other hand, for a better system performance,

we can take the peak time as $t_{p,c} = 0.015$s, which leads to the damping ratio and natural frequency to be 0.80 and 350 rad/s, respectively.

To achieve the desired performance requirements, consider the characteristic equation of the second order transfer function

$$(s^2 + 2\zeta w_n s + w_n^2) = 0 \qquad \textbf{(3.1.1.3)}$$

Now, PI controller is designed by

$$V_c(t) = k_{p,c}(I_r(t) - I_c(t)) + k_{i,c}\int (I_r(t) - I_c(t))dt \qquad \textbf{(3.1.1.4)}$$

The Laplace transform of Equation (3.1.1.4) is

$$V_c(s) = \left(k_{p,c} + \frac{k_{i,c}}{s}\right)(I_r(s) - I_c(s)) \qquad \textbf{(3.1.1.5)}$$

Substituting Equation (2.1.1.2) into Equation (3.1.1.5), we can obtain the closed-loop transfer function for the electrical part as

$$T_c(s) = \frac{I_c(s)}{I_r(s)} = \frac{K_c(k_{p,c}s + k_{i,c})}{\tau_c s^2 + (K_c k_{p,c} + 1)s + K_c k_{i,c}} \qquad \textbf{(3.1.1.6)}$$

By using pole placement method, which compares the characteristic equation of closed-loop system (3.1.1.6) with the desired characteristic equation (3.1.1.3) to find the appropriate control gains, $k_{p,c}$ and $k_{i,c}$, as

$$k_{p,c} = \frac{2\zeta w_n \tau_c - 1}{K_c},\ k_{i,c} = \frac{w_n^2 \tau_c}{K_c} \qquad \textbf{(3.1.1.7)}$$

3.1.2 High-Gain Sliding Mode Controller

The coil inductance value depends on the ball position, but it is taken as a constant to simplify analysis and designs. However, this assumption results in a parameter uncertainty in the electrical part. High-gain sliding mode controller (SMC) is designed for the inner electrical part of magnetic levitation system to control the coil current due to its fast response and robustness features.

To design SMC, first a sliding surface, s, can be designed for the first order electrical part as

$$s = I_r - I_c \tag{3.1.2.1}$$

Thus, the time-derivative of Equation (3.1.2.1), $\dot{s}$, is obtained as

$$\dot{s} = \dot{I}_r - \dot{I}_c = \dot{I}_r + \frac{R_c + R_s}{L_c} I_c - \frac{1}{L_c} V_c \tag{3.1.2.2}$$

To achieve a sliding mode, i.e., $s = \dot{s} = 0$, the equivalent coil voltage, V_{eq}, can be found as

$$V_{eq} = \frac{\tau_c}{K_c}[\dot{I}_r + \frac{1}{\tau_c} I_c] \tag{3.1.2.3}$$

The control input for the electrical part of the magnetic levitation system is

$$V_c = V_{eq} + V_0 \,\mathrm{sat}(s) \tag{3.1.2.4}$$

where

$$\mathrm{sat}(s/\varepsilon) = \begin{cases} \mathrm{sgn}(s/\varepsilon), & if \quad |s/\varepsilon| \geq 1 \\ s/\varepsilon \ , & if \quad |s/\varepsilon| < 1 \end{cases} \tag{3.1.2.5}$$

where $\varepsilon > 0$.

Because the electrical part has the first-order dynamics, it is also possible to design the controller as

$$V_c = V_0 \,\mathrm{sat}(s) \tag{3.1.2.6}$$

The saturation function, sat(.), is used to eliminate chattering on the system output. The stability of the SMC is given with the reachability condition, $s\dot{s} < 0$, which is obtained from the Lyapunov stability theorem [20,21]. It is similar to the analysis given in Section 3.1.4, and the gain parameter, V_0 can be found as bigger than zero ($V_0 > 0$) for satisfying the stability.

3.1.3 Process Sliding Mode Controller

A process sliding mode controller (PSMC) is designed for the inner electrical part of the magnetic levitation system to control the coil current

because the SMC can supply fast response to the inner control current loop. Moreover, the coil inductance value depends on the ball position, but it is assumed as a constant to simplify analysis and designs, so there exists a parameter uncertainty. Similar to the high-gain SMC, the PSMC can also eliminate this parameter uncertainty. In addition, since the effects of inductance related uncertainties can cause chattering, the PSMC can be designed to minimize possibility of the chattering.

To design PSMC, first a sliding surface, *s*, can be designed for the first order inner electrical part as

$$s = I_r - I_c \qquad \textbf{(3.1.3.1)}$$

The voltage V_c as the control input of the magnetic levitation can be designed as [24,25]

$$V_c = \alpha |s|^{0.5} \operatorname{sat}(s) + \beta \int |s|^{0.5} \operatorname{sat}(s) dt \qquad \textbf{(3.1.3.2)}$$

The saturation function, sat(.), is defined in Equation (3.1.2.5) and is used to eliminate chattering on the system output. The stability of the controller is similar to the analysis given in Section 3.1.4. For stability, the appropriate gains, α and β, must be positive. Since a boundary layer approach (sat(.) function) is used in the controller design, the trajectory reaches a small ultimate bound set in finite time. This means that the tracking error also stays around the origin, but usually not in the origin.

3.1.4 Sliding Mode Control Designs under Varying Coil Inductance

The coil inductance is dependent on the ball position, x_b, can be again written as

$$L_c(x_b) = L_1 + \frac{K_m}{x_b} \qquad \textbf{(3.1.4.1)}$$

Thus, by substituting Equation (3.1.4.1) into Equation (2.1.2.2) and applying chain rule, we can write the stable and nonlinear electrical model again as

$$\frac{dI_c}{dt} = -\frac{R_c + R_s}{L_c} I_c + \frac{K_m}{L_c} \frac{I_c \dot{x}_b}{x_b^2} + \frac{1}{L_c} V_c \qquad \textbf{(3.1.4.2)}$$

The sliding surface is again defined by

$$s = I_r - I_c \qquad \textbf{(3.1.4.3)}$$

Thus, the time-derivative of Equation (3.1.4.3), $\dot{s}$, is obtained as

$$\dot{s} = \dot{I}_r - \dot{I}_c = \dot{I}_r + \frac{R_c + R_s}{L_c} I_c - \frac{K_m}{L_c} \frac{I_c \dot{x}_b}{x_b^2} - \frac{1}{L_c} V_c \qquad \textbf{(3.1.4.4)}$$

During the sliding mode, i.e., $s = \dot{s} = 0$, the equivalent coil voltage, V_{eq}, can be found as

$$V_{eq} = L_c[\dot{I}_r + \frac{R_c + R_s}{L_c} I_c(t) - \frac{K_m}{L_c} \frac{I_c(t)}{x_b^2} \dot{x}_b] \qquad \textbf{(3.1.4.5)}$$

By using this equivalent value, the SMC controller can be designed as

$$V_c = V_{eq} + V_0 \,\mathrm{sat}(s) \qquad \textbf{(3.1.4.6)}$$

Or we can also design high-gain SMC (Equation (3.1.2.6)) and PSMC (Equation (3.1.3.2)) controllers to get desirable results.

For stability analysis of the SMC controllers, we must show that the controllers satisfy the reachability condition $s\dot{s} < 0$. If we consider the PSMC controller under varying coil inductance, the stability of the PSMC must be satisfied for selected appropriate gains, α and β. By considering the electrical model given in Equation (3.1.4.2), sliding surface given in Equation (3.1.4.3), and controller given in Equation (3.1.3.2), stability analysis of the proposed SMC can be carried out as follows. First, if a positive definite Lyapunov function is defined by

$$V = \frac{1}{2} s^2 + \frac{1}{2} u_1^2 \qquad \textbf{(3.1.4.7)}$$

where $\dot{u}_1 = \beta |s|^{0.5} \,\mathrm{sat}(s)$. Then its derivative must be negative definite for stability,

$$\dot{V} = s\left(\dot{I}_r + \frac{R_c + R_s}{L_c} I_c - h(x_b, \dot{x}_b, I_c) - \frac{1}{L_c} V_c \right) + u_1 \dot{u}_1 \qquad \textbf{(3.1.4.8)}$$

where $h(x_b, \dot{x}_b, I_c) = \frac{K_m}{L_c} \frac{I_c \dot{x}_b}{x_b^2}$. From Equation (3.1.2.5), it is clear that the controller consists of outer and inner parts. For the outer part of the controller, i.e. for $|s| \geq \varepsilon$, we have

$$\dot{V} = s\left(\dot{I}_r + \frac{R_c + R_s}{L_c} I_c - h(x_b, \dot{x}_b, I_c) - \frac{\alpha}{L_c} |s|^{1/2} \operatorname{sgn}(s) \right) + \varphi_0 \qquad \textbf{(3.1.4.9)}$$

where the function φ_0 can be written as

$$\begin{aligned} \varphi_0 &= -u_1 s / L_c + \beta u_1 |s|^{1/2} \operatorname{sgn}(s) \\ &= -\beta u_1 s \left(1 - \frac{1}{|s|^{1/2}} \right) \\ &= -\gamma \beta u_1 s \end{aligned} \qquad \textbf{(3.1.4.10)}$$

where $0 \leq \gamma < 1$ and it is assumed that $\beta = 1 / L_c$ for simplicity. Now the derivative of the Lyapunov function given in Equation (3.1.4.9) satisfies the inequality

$$\begin{aligned} \dot{V} &\leq \left(|\dot{I}_r| + \frac{R_c + R_s}{L_c} I_c + |h(x_b, \dot{x}_b, I_c)| + \gamma \beta |u_1| - \frac{\alpha}{L_c} |s|^{1/2} \right) |s| \\ &= -\left(\frac{\alpha}{L_c} |s|^{1/2} - \mu \right) |s| \end{aligned} \qquad \textbf{(3.1.4.11)}$$

where $\mu = |\dot{I}_r| + I_c (R_c + R_s) / L_c + |h(x_b, \dot{x}_b, I_c)| + \gamma \beta |u_1|$. Since $|s| \geq \varepsilon$, if we choose $\alpha > L_c \mu / \sqrt{\varepsilon}$, then $\dot{V} < 0$. That is to say, whenever $|s| \geq \varepsilon$, $|s(t)|$ will strictly decrease until it reaches the set $|s| < \varepsilon$ in finite time and remains inside the set subsequently. For the inner part of the controller, i.e. inside the set $|s| < \varepsilon$ the derivative of the Lyapunov function can similarly be written as

$$\dot{V} = s\left(\dot{I}_r + \frac{R_c + R_s}{L_c} I_c - h(x_b, \dot{x}_b, I_c) - \frac{\alpha}{L_c} |s|^{1/2} s / \varepsilon \right) + \varphi_1 \qquad \textbf{(3.1.4.12)}$$

with

$$\begin{aligned}\varphi_1 &= -u_1 s / L_c + \beta u_1 |s|^{1/2} s / \varepsilon \\ &= -\beta u_1 s\left(1 - |s|^{1/2} / \varepsilon\right) \\ &= -\gamma_1 \beta u_1 s\end{aligned} \qquad \textbf{(3.1.4.13)}$$

where $0 < \gamma_1 < 1$ and again it is assumed that $\beta = 1/L_c$ for simplicity. Finally we get

$$\begin{aligned}\dot{V} &\le \bar{\mu}|s| - \frac{\alpha}{\varepsilon L_c}|s|^{5/2} \\ &\le -(1-\theta)\frac{\alpha}{\varepsilon L_c}|s|^{5/2}\end{aligned} \qquad \textbf{(3.1.4.14)}$$

where $0 < \theta < 1$ and $\bar{\mu} = |\dot{I}_r| + I_c(R_c + R_s)/L_c + |h(x_b, \dot{x}_b, I_c)| + \gamma_1 \beta |u_1|$. The inequality Equation (3.1.4.14) is satisfied for all

$$|s| \ge \left(\frac{\varepsilon L_c \bar{\mu}}{\theta \alpha}\right)^{2/3} \qquad \textbf{(3.1.4.15)}$$

Hence, the trajectory reaches the ultimate bound set $\Sigma = \left\{|s| < \left(\varepsilon\bar{\mu}/(\theta\alpha K_c)\right)^{2/3}, |s| < \varepsilon\right\}$ in finite time. This means that the tracking error also stays around the origin, but not in the origin in general. Consequently the practical stability of the proposed controller Equation (3.1.3.2) is guaranteed for the given ultimate bound. It is clear that the stability condition is obtained as $\alpha > L_c \mu / \sqrt{\varepsilon}$. However, the stability analysis does not provide a straightforward condition for the control gain β, and thus it may be selected arbitrarily to get a satisfying steady-state response.

Robustness of the Sliding Mode Current Controller: From Equation (3.1.4.4), the differential equation of the sliding surface including uncertainties can be written as

$$\dot{s} = \dot{I}_r + \delta_0 I_c - \delta_1 V_c - h(x_b, \dot{x}_b, I_c) \qquad \textbf{(3.1.4.16)}$$

where $h(\cdot)$ represents the nonlinear part of the model Equation (3.1.4.2), considered as a bounded disturbance, $|h(x_b, \dot{x}_b, I_c)| \le \mu_0$, $\delta_0 = \frac{R_c + R_s}{L_c} + \Delta_0 > 0$,

and $\delta_1 = \frac{1}{L_c} + \Delta_1 > 0$ with bounded inductance related uncertainties Δ_0 and Δ_1.

By using Lyapunov stability theorem as described above, one can found similar stability conditions,

$$\alpha > L_c\tilde{\mu}/(1+L_c\Delta_1)\,, \quad \varepsilon > |s| \geq \left(\frac{\varepsilon L_c\hat{\mu}}{\theta\alpha(1+L_c\Delta_1)}\right)^{2/3} \qquad \textbf{(3.1.4.17)}$$

where $\tilde{\mu} \geq \mu$ and $\hat{\mu} \geq \bar{\mu}$ due to the bounds of uncertainties and disturbance. Consequently, the practical stability of the system can be guaranteed under bounded uncertainties.

3.2 Design of the Outer Controllers

The outer controller is designed to control the ball position, x_b, for the mechanical part of magnetic levitation system. The coil current is varied appropriately to control the position of the ball of the mechanical part of the system. The nonlinear mechanical part has much slower response than the electrical part of the system. In this context, sliding mode and PID (Proportional, Integral and Derivative) based controllers are considered for controlling the ball position. For controlling the outer loop, the PI plus velocity (PIV) controller, sliding mode controller (SMC) and integral sliding mode controller (ISMC) will be designed to control the ball position of the magnetic levitation system as shown in Fig. 3.2.1. The coil current limiter is used to limit 0-3A the coil current value due to the specification of magnetic levitation system. Maximum current value is 3A and minimum current value is 0A because of the steel ball resting at the post.

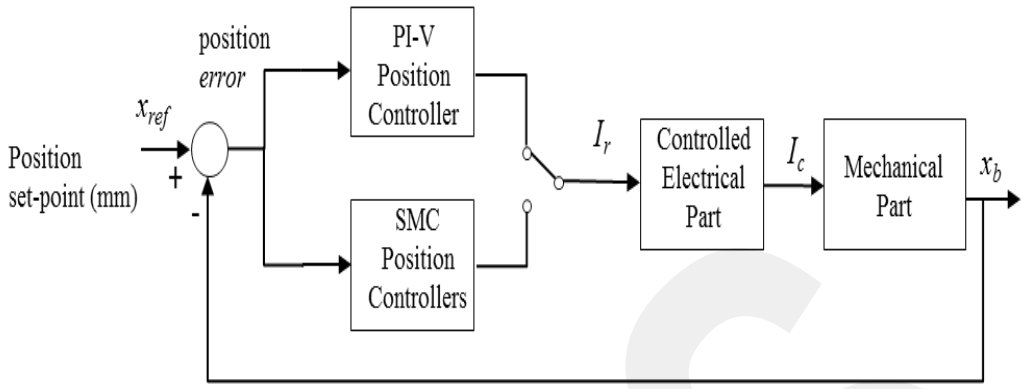

Figure 3.2.1 Block diagram of the outer position loop.

The magnetic levitation system consists of the open-loop unstable mechanical part and highly nonlinear dynamics, and existence of parameter uncertainties due to the assumption of the coil inductance value as a constant in addition to dynamic disturbances around the linear operating point (x_{b0}, I_{c0}). So, PI-V controller with set point weighting, sliding mode controller and integral sliding mode controller are designed to control the ball position for the mechanical part of magnetic levitation system to deal with these problems. I primarily designed the SMC to control the ball position for the outer mechanical part to track the reference position precisely.

3.2.1 PI plus Velocity Controller

The proportional plus integral plus velocity (PI-V) controller is designed and tuned with pole placement by using convenient specifications to control the ball position of the outer mechanical part of the magnetic levitation system. The magnetic levitation system consists of highly nonlinear dynamics, so includes very noises. In the controller design, the velocity (V) controller which does not consist of derivative of the reference position is designed to eliminate noise by filtering the ball position. A second-order derivative filter is designed as

$$G_d(s) = \frac{\omega_d^2 s}{s^2 + 2\zeta_d \omega_d s + \omega_d^2} \quad \textbf{(3.2.1.1)}$$

where the filter parameters ζ_d and ω_d should be selected appropriately in order not to eliminate system dynamics (e.g., 30 times faster than the plant dynamics). In addition, feed-forward is attached to the controller to track the reference position due to having capable of elimination disturbances around operating point. Thus, the PI-V controller with feed forward is designed as

$$I_r(t) = k_{p,b}(x_{ref}(t) - x_b(t)) + k_{i,b}\int (x_{ref}(t) - x_b(t))dt - k_{v,b}\frac{dx_b(t)}{dt} + K_{ff,b}x_{ref}(t) \quad \textbf{(3.2.1.2)}$$

where $K_{ff,b}$ is the feed forward gain parameter. At equilibrium, $x_{ref} = x_b = x_{b0}$, thus the ball position control presented in Equation (3.2.1.2) is obtained as

$$I_r = K_{ff,b}x_{b0} \quad \textbf{(3.2.1.3)}$$

At the equilibrium current, $I_r = I_{c0}$, so the feed forward gain is obtained as

$$K_{ff,b} = \frac{I_{c0}}{x_{b0}} \quad \textbf{(3.2.1.4)}$$

The operating point of the system is assumed to be x_{b0}=6mm and I_{c0}=0.86A and so $K_{ff,b}$ can be found as 138.6 A/m.

The feed forward gain ($K_{ff,b}$) can be converted to the set point weighting (b_{sp}) as follows

$$\left(b_{sp}x_{ref} - x_b\right)k_{p,b} = x_{ref}K_{ff,b} + \left(x_{ref} - x_b\right)k_{p,b} \quad \textbf{(3.2.1.5)}$$

Hence,

$$b_{sp} = \frac{K_{ff,b}}{k_{p,b}} + 1 \quad \textbf{(3.2.1.6)}$$

The objective of set point weighting is to compensate for the gravitational bias. When the PI-V controller compensates for dynamic disturbances around the linear operating point (x_{b0}, I_{c0}) the set point weighting eliminates the changes in the force created due to gravitational bias. Hence, the set point weighting is applied to the proportional controller to have a good steady-state response.

Now, the PI-V with set point weighting can be designed by

$$I_r(t) = k_p(b_{sp}x_{ref}(t) - x_b(t)) + k_i\int(x_{ref}(t) - x_b(t))dt - k_v\frac{dx_b(t)}{dt} \quad \textbf{(3.2.1.7)}$$

The Laplace transform of Equation (3.2.1.7) is

$$I_r(s) = k_p b_{sp} X_{ref}(s) - k_p X_b(s) + \frac{k_i}{s}\left(X_{ref}(s) - X_b(s)\right) - k_v s X_b(s) \quad \textbf{(3.2.1.8)}$$

Thus, the closed-loop transfer function can be written as

$$T_b(s) = \frac{X_b(s)}{X_{ref}(s)} = \frac{I_r(s)}{X_{ref}(s)}\frac{V_c(s)}{I_r(s)}\frac{I_c(s)}{V_c(s)}\frac{X_b(s)}{I_c(s)} = \frac{I_r(s)}{X_{ref}(s)}\frac{V_c(s)}{I_r(s)}G_c(s)G_b(s) \quad \textbf{(3.2.1.9)}$$

With the assumption $I_r(s) = I_c(s)$ as the inner control loop controls the coil current, namely,

$$\frac{V_c(s)}{I_r(s)}G_c(s) = 1 \quad \textbf{(3.2.1.10)}$$

Thus, the closed loop position transfer function is

$$T_b(s) = \frac{X_b(s)}{X_{ref}(s)} = \frac{I_r(s)}{X_{ref}(s)}G_b(s) \quad \textbf{(3.2.1.11)}$$

Substituting Equation (3.2.1.8) into Equation (3.2.1.11), we can obtain

$$T_b(s) = \frac{2gx_{b0}(k_p s + k_i + k_p s(b_{sp} - 1))}{-I_{c0}x_{b0}s^3 + 2gx_{b0}k_v s^2 + 2g(x_{b0}k_p + I_{c0})s + 2gx_{b0}k_i} \quad \textbf{(3.2.1.12)}$$

Now, if we define desired performance requirements for the ball position control as

1) Percent overshoot (PO) ≤ 5%,
2) Settling time (t_s) ≤ 0.3s,

then these performance requirements can be used to get desired characteristic equation of the system, that is to say,

$$(s^2 + 2\zeta w_n s + w_n^2)(s + p_0) = 0 \quad \textbf{(3.2.1.13)}$$

The damping ratio is found as ζ=0.69 from Equation (3.1.1.1) and the settling time is given by

$$t_s = \frac{4}{\zeta w_n} \quad \textbf{(3.2.1.14)}$$

Thus, the natural frequency can be found as ω_n=19.3 rad/s from Equation (3.2.1.14) by providing the desired settling time. The third pole (p_0) location is

selected as -40 by taking into account the feature [p_0<dominant pole]. Moreover, the third pole should not be taken as very small. Otherwise, the control gains can increase a lot. The pole p_0 is usually selected as 2-5 times the dominant pole in order to obtain good feedback responses.

Consequently, by comparing the characteristic equation of closed-loop system (3.2.1.12) with the desired characteristic equation (3.2.1.13), the controller gains used in PIV controller design are found as

$$k_p = -\frac{(2p_0\zeta\omega_n x_{b0} + \omega_n^2 x_{b0} + 2g)I_{c0}}{2x_{b0}},\ k_i = -\frac{p_0\omega_n^2 I_{c0}}{2g},$$
$$k_v = -\frac{(p_0 + 2\zeta\omega_n)I_{c0}}{2g},\ b_{sp} = 1 + \frac{I_{c0}}{k_p x_{b0}} \quad \textbf{(3.2.1.15)}$$

3.2.2 Integral Sliding Mode Controller

The sliding mode based controller is designed as the outer controller to control the ball position of the magnetic levitation system. Here, in the outer controller design for the magnetic levitation system, $I_r = I_c$ is assumed to decrease the complexity due to the inner current control loop. Thus, we focus on the mechanical part of the system to control the ball position.

Both SMC and integral SMC as the outer controller are separately designed to control the ball position for the mechanical part of magnetic levitation system. For the second-order mechanical system, a sliding surface, s_1, can be designed as

$$s_1 = \dot{e} + \lambda e \quad \textbf{(3.2.2.1)}$$

where $e = x_r - x_b$ and $\lambda > 0$. However, under this sliding surface, I have found that the ball position does not truly track the reference position and includes high error (position error) and unsatisfactory settling time in numerical and experimental results. Thus, an integral part is added to the sliding surface for a precise reference tracking. Integral SMC (ISMC) design for the outer controller

the new sliding surface, s_1, can be designed for the second-order mechanical system as

$$s_1 = \dot{e} + \lambda e + \lambda_0 \int e dt \qquad \textbf{(3.2.2.2)}$$

where $e = x_r - x_b$, $\lambda > 0$ and $\lambda_0 > 0$. In addition, the second-order system from Equation (2.3.3) is obtained as

$$\ddot{x}_b - w_b^2 x_b + K_b w_b^2 i_c = 0 \qquad \textbf{(3.2.2.3)}$$

Thus, the time-derivative of Equation (3.2.2.2), $\dot{s}_1$, is obtained as

$$\dot{s}_1 = \ddot{x}_r - w_b^2 x_b + K_b w_b^2 i_c + \lambda(\dot{x}_r - \dot{x}_b) + \lambda_0(x_r - x_b) \qquad \textbf{(3.2.2.4)}$$

During sliding mode, i.e., $s_1 = \dot{s}_1 = 0$, the equivalent current, i_{eq}, can be obtained as follows

$$i_{eq} = -\frac{1}{K_b w_b^2}\left[\ddot{x}_r - w_b^2 x_b + \lambda(\dot{x}_r - \dot{x}_b) + \lambda_0(x_r - x_b)\right] \qquad \textbf{(3.2.2.5)}$$

The equivalent current controller is necessary to keep the system trajectory on the sliding surface and to reduce chattering on the system output. Therefore, the control input to the mechanical part of the magnetic levitation system can be designed in ISMC design as

$$i_c = i_{eq} + i_0 \text{sat}(s_1) \qquad \textbf{(3.2.2.6)}$$

where

$$\text{sat}(s_1/\varepsilon) = \begin{cases} \text{sgn}(s_1/\varepsilon), & if \quad |s_1/\varepsilon| \geq 1 \\ s_1/\varepsilon\ , & if \quad |s_1/\varepsilon| < 1 \end{cases} \qquad \textbf{(3.2.2.7)}$$

where $\varepsilon > 0$. The saturation function (sat(.)) is used to eliminate chattering on the system output.

The stability of the integral SMC must be satisfied for selected appropriate gain, i_0, (i.e., satisfying reachability condition $s_1\dot{s}_1 < 0$). By considering sliding surface given in Equation (3.2.2.2), the second-order linearized mechanical system given in Equation (3.2.2.3), the equivalent controller given in Equation (3.2.2.5), and the controller given in Equation

(3.2.2.6), stability analysis of the proposed SMC can be carried out as follows. First, if a positive definite Lyapunov function is defined by

$$V = \frac{1}{2} s_1^{\,2} \tag{3.2.2.8}$$

then its derivative must be negative definite for stability,

$$\begin{aligned} \dot{V} &= s_1 \dot{s}_1 \\ &= s_1 \left(\ddot{x}_r - w_b^2 x_b + K_b w_b^2 i_c + \lambda(\dot{x}_r - \dot{x}_b) + \lambda_0 (x_r - x_b) \right) \\ &= s_1 \left(K_b w_b^2 i_0 \, \mathrm{sat}(s_1) \right) \end{aligned} \tag{3.2.2.9}$$

From Equation (3.2.2.7), it is clear that the controller consists of outer and inner parts. For the outer part of the controller, i.e. for $|s_1 / \varepsilon| \geq 1$, we have

$$\begin{aligned} \dot{V} &= K_b w_b^2 i_0 s_1 \, \mathrm{sgn}(s_1 / \varepsilon) \\ &= K_b w_b^2 i_0 \frac{s_1 / \varepsilon}{|s_1 / \varepsilon|} s_1 \\ &= K_b w_b^2 i_0 \frac{s_1^2}{|s_1|} \\ &= K_b w_b^2 i_0 |s_1| \end{aligned} \tag{3.2.2.10}$$

Thus, the gain parameter, $i_0 < 0$, then $\dot{V} < 0$. That is to say, whenever $|s_1| \geq \varepsilon$, $|s_1(t)|$ will strictly decrease until it reaches the set $|s_1| < \varepsilon$ in finite time and remains inside the set subsequently. For the inner part of the controller, i.e. inside the set $|s_1 / \varepsilon| < 1$, the derivative of the Lyapunov function can similarly be written as

$$\begin{aligned} \dot{V} &= K_b w_b^2 i_0 s_1 \frac{s_1}{\varepsilon} \\ &= K_b w_b^2 i_0 \frac{s_1^2}{\varepsilon} \end{aligned} \tag{3.2.2.11}$$

Thus, the gain parameter is similarly obtained as $i_0 < 0$, then $\dot{V} < 0$. Consequently the practical stability of the proposed controller Equation (3.2.2.6) is guaranteed with $i_0 < 0$ condition. In addition, if we design only sliding mode controller for the linearized mechanical part, the integral part can be eliminated from the control input, i_c, in other word, $\lambda_0 = 0$. Note that it is possible to

increase system performance when we use $\ddot{e}$ instead of $\ddot{x}_r$ in the equivalent current controller.

Robustness of the Integral Sliding Mode Position Controller: From Equation (3.2.2.3), the second order linearized mechanical system including uncertainties can be written as

$$\ddot{x}_b - (w_b^2 + d_1(x_{b0}))x_b + (K_b w_b^2 + d_1(x_{b0}))i_c = 0 \qquad \textbf{(3.2.2.12)}$$

where it is assumed that $\left(K_b w_b^2 + d_1(x_{b0})\right) > 0$ and d_1 is the operating position variations as a function of x_{b0}. From Equation (3.2.2.4), the differential equation of the sliding surface including uncertainties can be written as

$$\dot{s}_1 = \ddot{x}_r - (w_b^2 + d_1)x_b + (K_b w_b^2 + d_1)i_c + \lambda(\dot{x}_r - \dot{x}_b) + \lambda_0(x_r - x_b) \quad \textbf{(3.2.2.13)}$$

For the Lyapunov function $V = s_1^2 / 2$, the time-derivative of the Lyapunov function is

$$\begin{aligned} \dot{V} &= s_1 \dot{s}_1 \\ &= s_1 \left(\ddot{x}_r - (w_b^2 + d_1)x_b + (K_b w_b^2 + d_1)i_c + \lambda(\dot{x}_r - \dot{x}_b) + \lambda_0(x_r - x_b) \right) \\ &= s_1 \left(-d_1 x_b + K_b w_b^2 i_0 \,\text{sat}(s_1) + d_1 i_{eq} + d_1 i_0 \,\text{sat}(s_1) \right) \end{aligned} \qquad \textbf{(3.2.2.14)}$$

For the outer part of the controller, i.e. for $|s_1| \geq \varepsilon$, by applying Cauchy-Schwarz inequality, we have

$$\begin{aligned} \dot{V} &= -d_1 x_b s_1 + d_1 i_{eq} s_1 + (K_b w_b^2 + d_1) i_0 \frac{s_1 / \varepsilon}{|s_1 / \varepsilon|} s_1 \\ &\leq |d_1 x_b||s_1| + |d_1 i_{eq}||s_1| + (K_b w_b^2 + d_1) i_0 |s_1| \\ &= \left(|d_1 x_b| + |d_1 i_{eq}| + (K_b w_b^2 + d_1) i_0 \right) |s_1| \end{aligned} \qquad \textbf{(3.2.2.15)}$$

Therefore, if $i_0 \leq -\left(|d_1 x_b| + |d_1 i_{eq}|\right) / (K_b w_b^2 + d_1)$, then it is guaranteed that the system trajectory will enter the inner boundary layer, $|s_1| < \varepsilon$, and stay there.

Note that for the maglev system under study, since the coil current works in the range of $0 \leq I_c \leq 3$, the extreme values of d_1 can be

$$|d_1| < K_b w_b^2 = \frac{2g}{I_{c0}} \quad \Rightarrow \quad |d_1| < 6.54. \qquad \textbf{(3.2.2.16)}$$

Chapter 4

Results

The cascade control design consists of an inner controller and an outer controller. The inner controller should give much fast response than the outer controller because the inner loop firstly controls the coil current, I_c. In this context, the selected convenient cascaded controls for numerical and experimental hardware in the loop (HIL) test studies are given as

1) The cascade PI-V with set point weighting (see Section 3.2.1) for the outer position loop plus PI (see Section 3.1.1) for the inner current loop controller.
2) The cascade PI-V with set point weighting for the outer position loop plus high-gain SMC (see Section 3.1.2) for the inner current loop controller.
3) The cascade PI-V with set point weighting for the outer position loop plus process SMC (PSMC) (see Section 3.1.3) for the inner current loop controller.
4) The cascade PI-V with set point weighting for the outer position loop plus equivalent SMC (eSMC) with varying inductance (see Section 3.1.4) for the inner current loop controller.
5) The cascade PI-V with set point weighting for the outer position loop plus process SMC (PSMC) with varying inductance (see Section 3.1.4) for the inner current loop controller.
6) The SMC (see Section 3.2.2) for the outer position loop plus PSMC for inner current loop controller.

7) The integral SMC (ISMC) (see Section 3.2.2) for the outer position loop plus PSMC for the inner current loop controller.
8) The ISMC for the outer position loop plus high-gain SMC for the inner current loop controller.
9) The ISMC for the outer position loop plus eSMC with varying inductance (see Section 3.1.4) for the inner current loop controller.
10) The ISMC for the outer position loop plus PSMC with varying inductance (see Section 3.1.4) for the inner current loop controller.

MATLAB/Simulink programs are used for all numerical and experimental results. It is assumed that the ball position varies between 8 to 10 mm ramp signals with a frequency of 0.25Hz. From the desired performance requirements (see Section 3.2.1), the controller should accomplish a desired ± 1mm square wave position set point. For some control designs, the sinusoidal reference tracking is also illustrated. The control parameter gains are obtained based on desired performance requirements and verified with numerical simulations. Moreover, the gains of SMC can be arranged with trial-error method via simulations in order to achieve design specifications. As the outer controllers, $k_{p,b} = -199.7$, $k_{i,b} = -633.2$, $k_{v,b} = -2.82$ and $b_{sp} = 0.35$ for PI-V controller with set-point weighting, $\lambda = 60$, $i_0 = -100$ and ε=100 for SMC, $\lambda = 60$, $\lambda_0 = 2000$, $i_0 = -50$ and ε=100 for ISMC. As the inner controllers and $k_{p,c} = 220$ and $k_{i,c} = 50430$ for PI controller, $V_0 = 50$ and $\varepsilon = 0.1$ for the inner high-gain SMC, $\alpha = 150$, $\beta = 50$ and $\varepsilon = 0.03$ for the inner PSMC, $V_0 = 500$ and $\varepsilon = 0.1$ for the inner equivalent SMC with varying inductance, $\alpha = 150$, $\beta = 50$ and $\varepsilon = 0.03$ for the inner PSMC with varying inductance.

For the selected some cascade controllers which are PI-V plus PI, PI-V plus PSMC, ISMC plus PSMC and ISMC plus eSMC with varying inductance, numerical and experimental results for 10 seconds are shown in this section. In addition, for all cascaded controllers, numerical and experimental results are given in tables for comparison.

4.1 PI-V plus PI Cascade Control

The PI-V controller with set point weighting for the mechanical part and PI controller for the electrical part are cascaded appropriately. The experimental hardware-in-the-loop (HIL) test and numerical simulation results of this cascade control for the magnetic levitation are provided in this section.

4.1.1 Numerical Simulations

The numerical simulation results of the cascade PI-V plus PI controller for 10 seconds are illustrated in Figs. 4.1.1.1-5. It is shown in Fig. 4.1.1.1 that the controller provides a desired tracking performance with a percent overshoot (around 2.3%). Figure 4.1.1.2 shows the coil current trajectory due to PI current controller. The coil current perfectly tracks the desired current, which makes the ball to follow the desired position. The coil voltage is shown in Fig. 4.1.1.3. The tracking error shown in Fig. 4.1.1.4 is the difference between actual trajectory and reference trajectory. The tracking error has little short transient response which satisfies the required settling time, and about 0.22mm (2.2% overshoot) in the simulations. Fig. 4.1.1.5 shows that the current error goes to almost zero in a short time and stays around zero for all subsequent times.

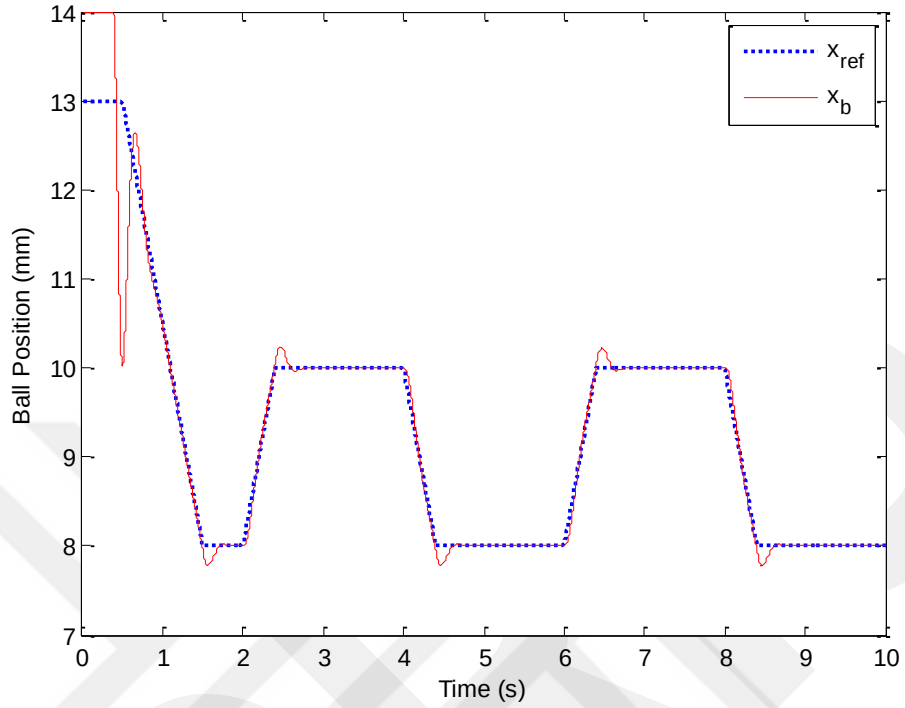

Figure 4.1.1.1 Ball position trajectory for PI-V plus PI.

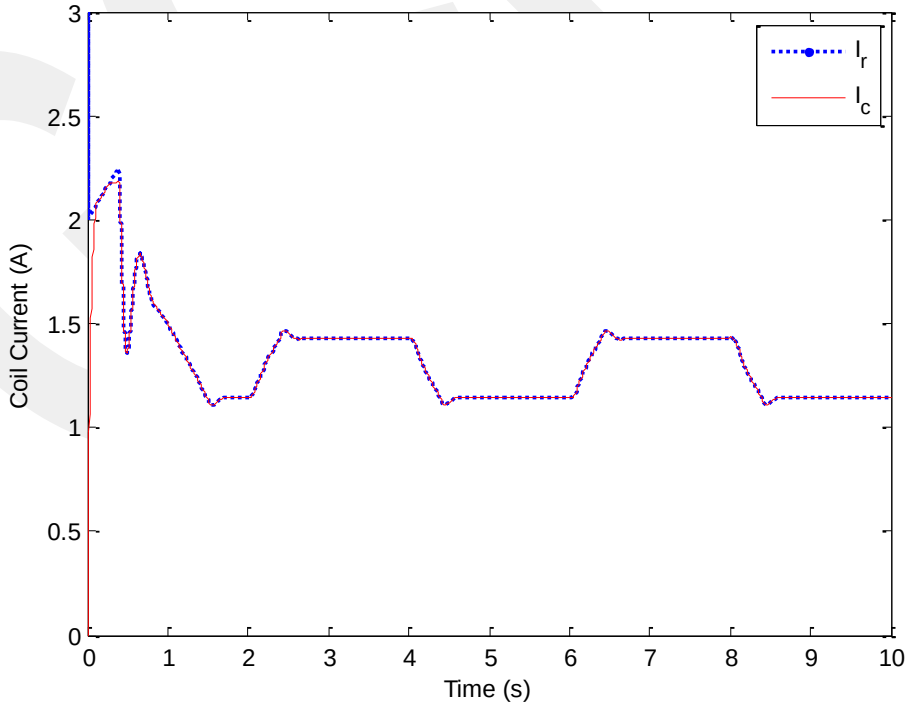

Figure 4.1.1.2 Coil current response for PI-V plus PI.

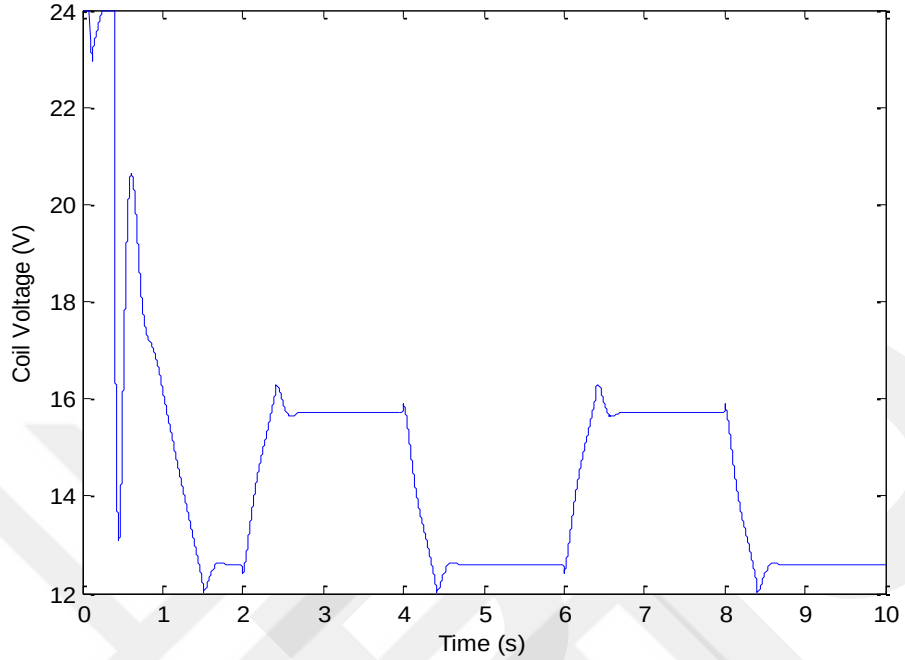

Figure 4.1.1.3 Coil voltage response for PI-V plus PI.

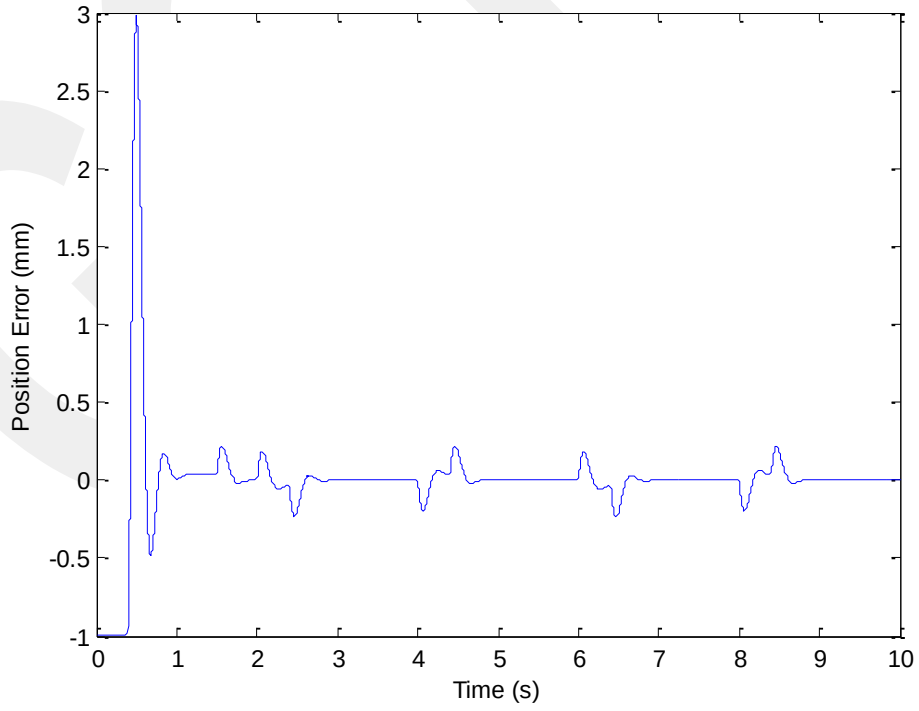

Figure 4.1.1.4 Position tracking error for PI-V plus PI.

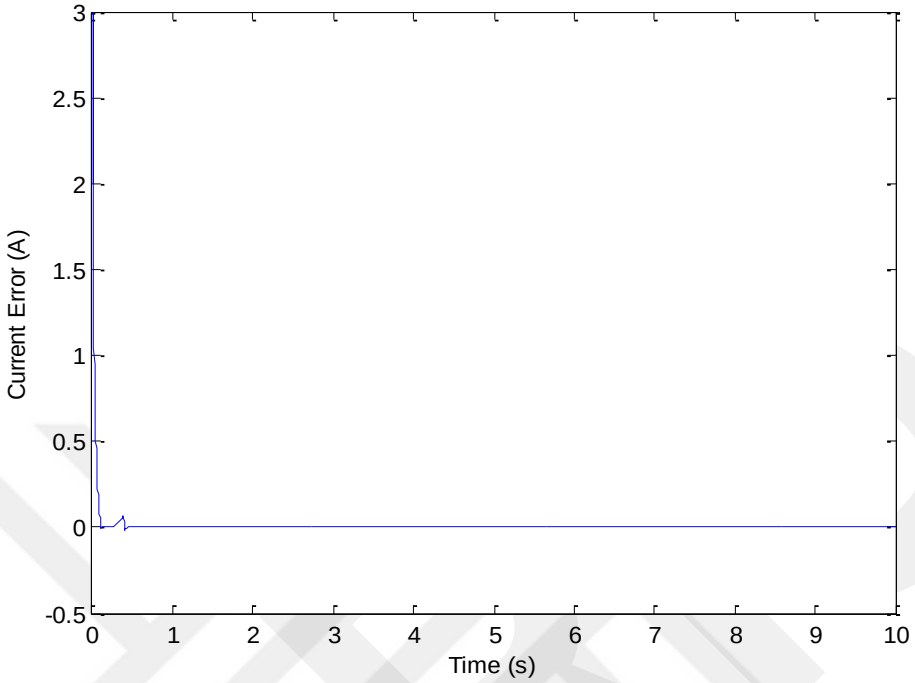

Figure 4.1.1.5 Current tracking error for PI-V plus PI.

4.1.2 Experimental Results

The experimental results of the cascade PI-V plus PI controller for 10 seconds are shown in Figs. 4.1.2.1-5. Figure 4.1.2.1 shows that the controller holds the ball during startup and follows the reference position trajectory thereafter. The small oscillations around the reference point are due to the effects of sampling time, measurement error and noise. In addition, the ball sways right and left rather than staying vertically as the photo detector does not exactly measure the ball position because of circularly ball.

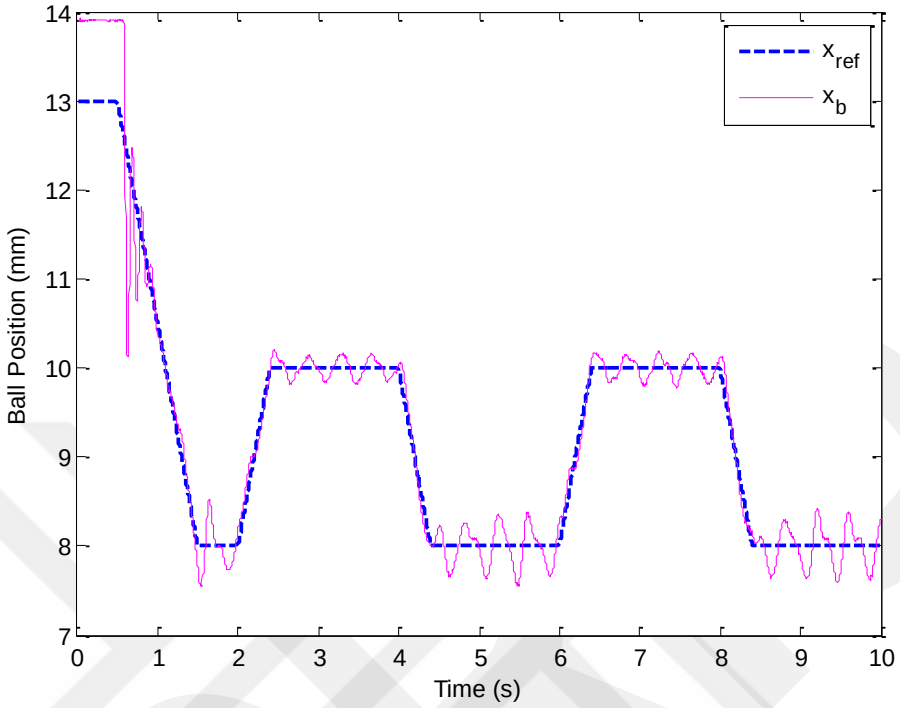

Figure 4.1.2.1 Experimental ball position trajectory for PI-V plus PI.

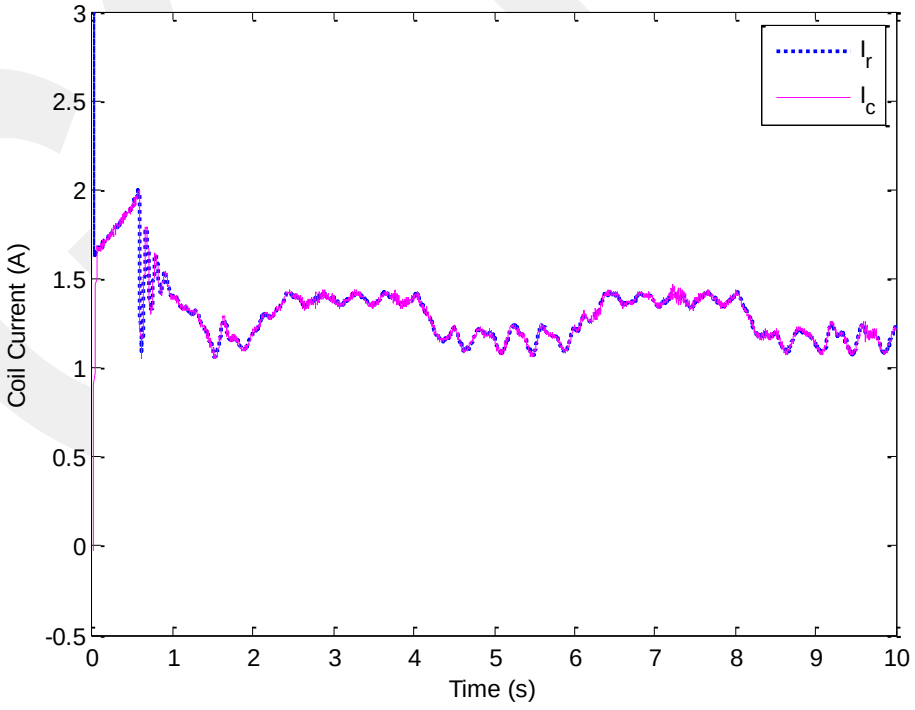

Figure 4.1.2.2 Experimental coil current response for PI-V plus PI.

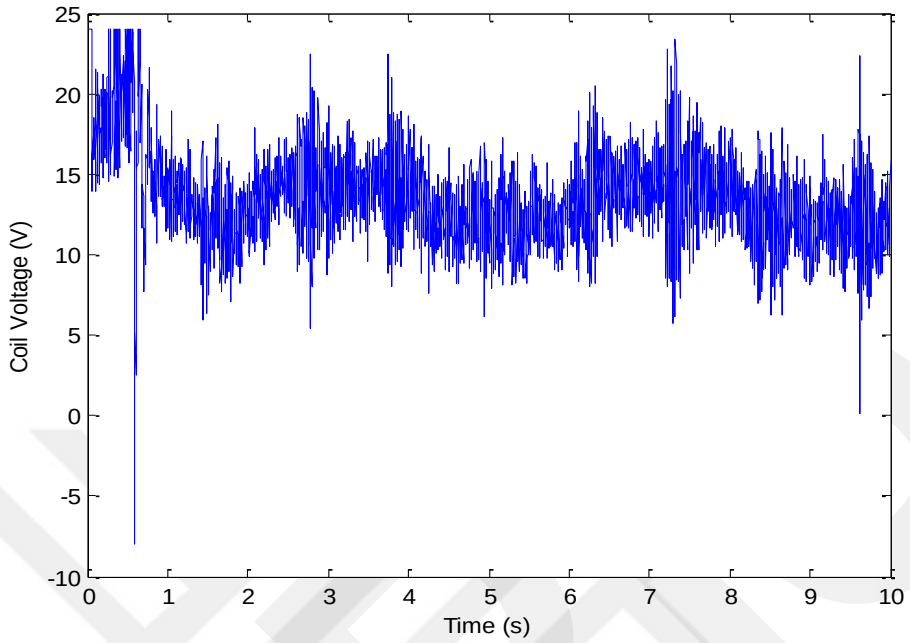

Figure 4.1.2.3 Experimental coil voltage response for PI-V plus PI.

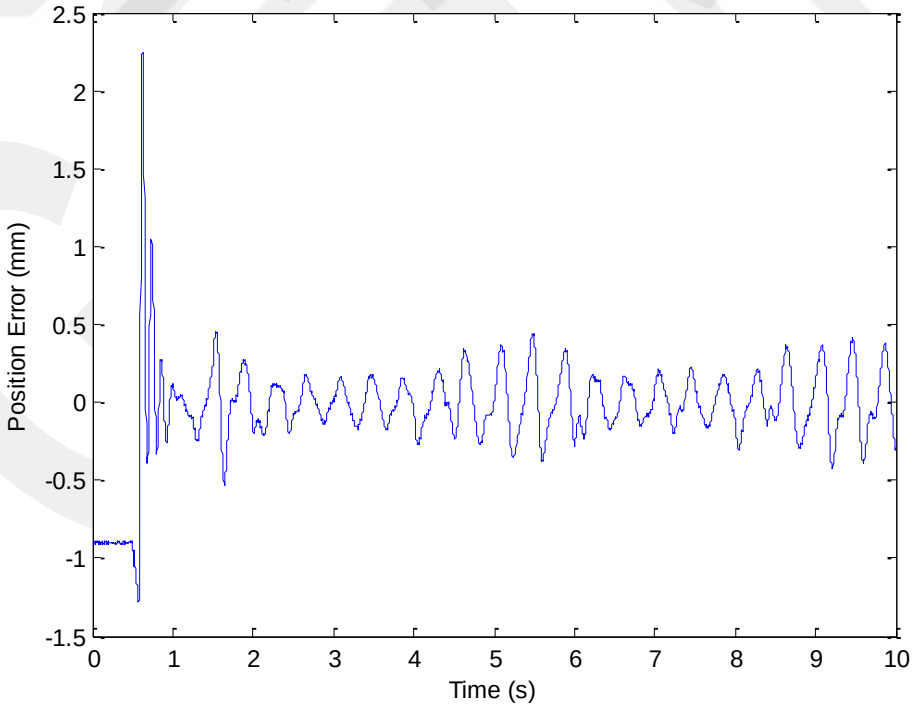

Figure 4.1.2.4 Experimental position tracking error for PI-V plus PI.

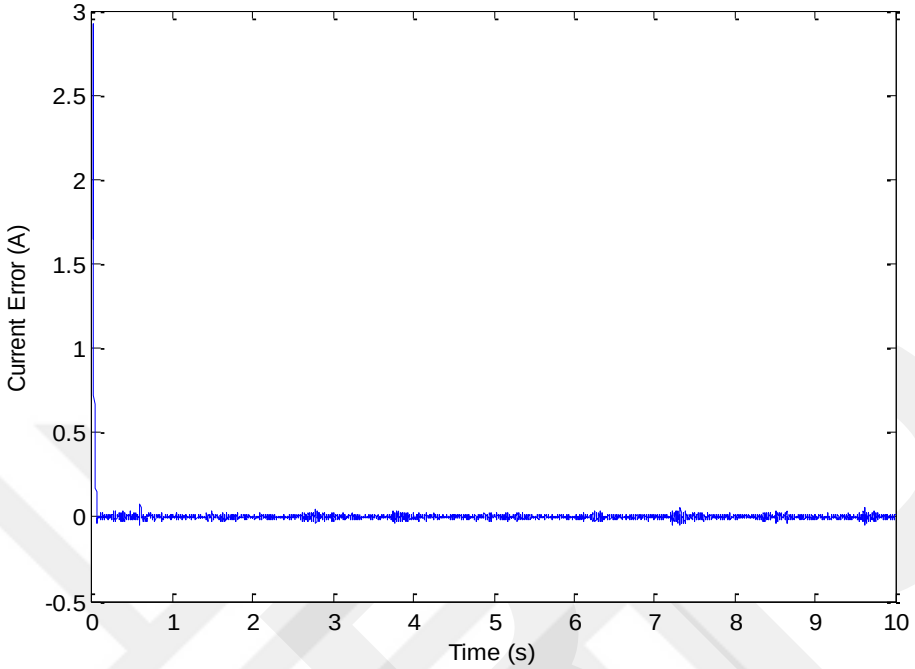

Figure 4.1.2.5 Experimental current tracking error for PI-V plus PI.

Figure 4.1.2.2 shows the coil current trajectory. PI current controller provides a satisfactory tracking performance. The response of the coil voltage is shown in Fig. 4.1.2.3. The average voltage supply is around 14V during steady-state. The position tracking error is shown in Fig. 4.1.2.4. It is clear that the position error is limited about 0.23mm during steady-state which satisfies desired requirements. Figure 4.1.2.5 shows the current tracking error. It is seen that the current error reaches almost zero with 0.03A error in a short time and stays around zero thereafter.

4.2 PI-V plus Process SMC Cascade Control

The PI-V controller with set point weighting for the mechanical part and the process SMC for the electrical part are cascaded appropriately. The experimental hardware-in-the-loop (HIL) test and numerical simulation results of this cascade control for the magnetic levitation are provided in this section.

4.2.1 Numerical Simulations

The numerical simulation results of the cascade PI-V plus process SMC controller are shown in Figs. 4.2.1.1-5. It is illustrated in Fig. 4 that the controller provides a desired tracking performance with a little overshoot (around 2%). Figure 4.2.1.2 shows the coil current trajectory of the SMC current controller in which the coil current perfectly tracks the desired current, which makes the ball to follow the reference trajectory. The control signal, i.e., coil voltage, is shown in Fig. 4.2.1.3. Smooth voltage and current signals are observed in the simulations. The tracking error, which is the difference between actual trajectory and reference trajectory, is shown in Fig. 4.2.1.4. The tracking error has little short transient response which satisfies the required settling time, and about 0.2mm (2% overshoot) in the simulations. Fig. 4.2.1.5 shows that the sliding surface, *s*, (or current error) goes to almost zero in a short time and stays around zero for all subsequent times.

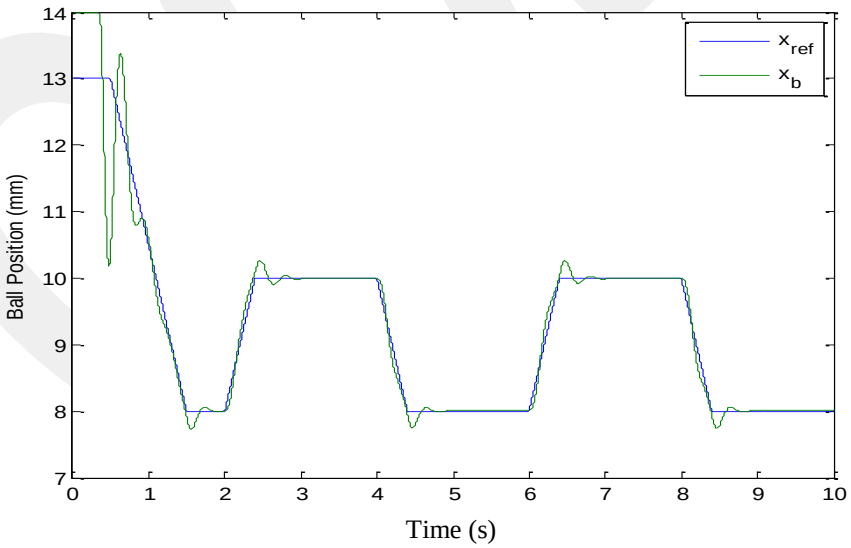

Figure 4.2.1.1 Ball position trajectory for PI-V plus PSMC.

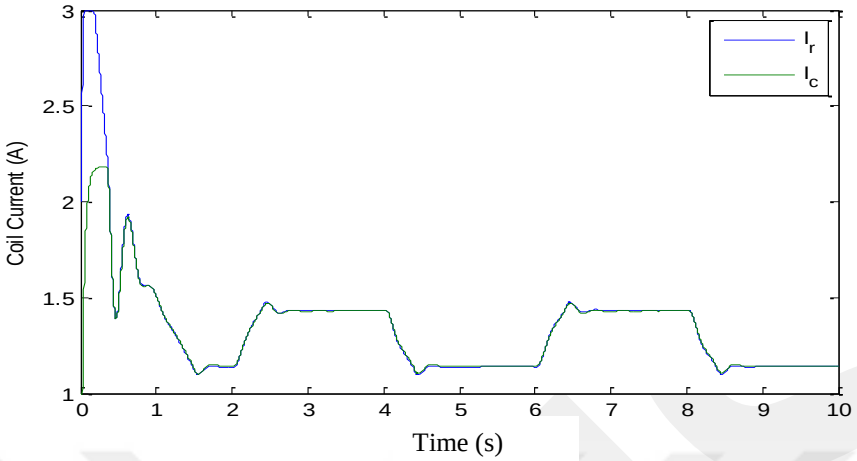

Figure 4.2.1.2 Coil current response for PI-V plus PSMC.

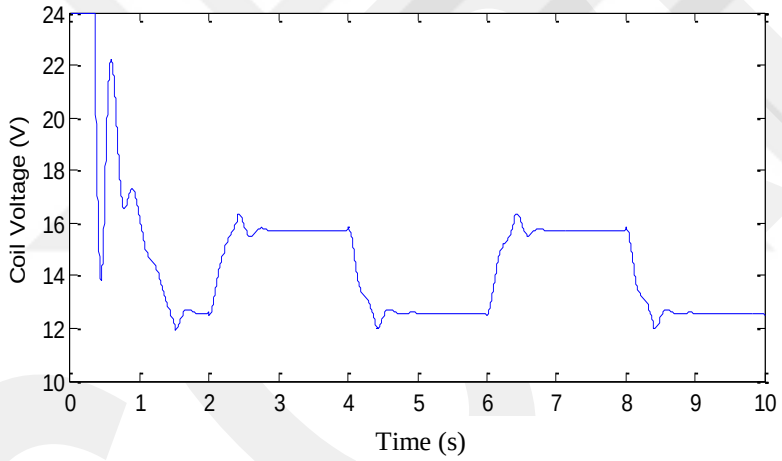

Figure 4.2.1.3 Coil voltage response for PI-V plus PSMC.

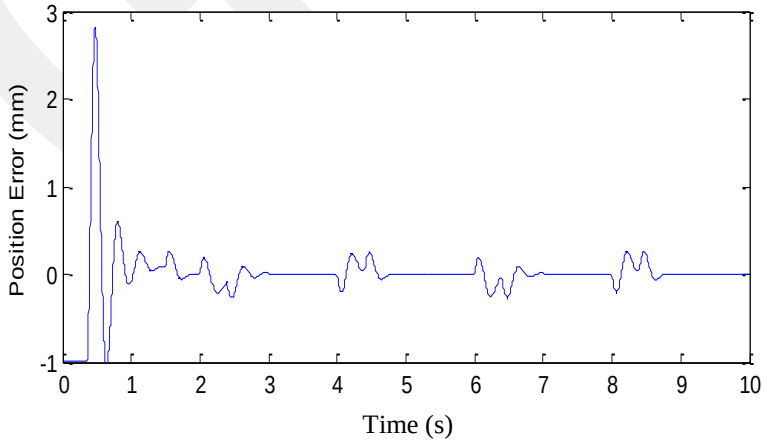

Figure 4.2.1.4 Position tracking error for PI-V plus PSMC.

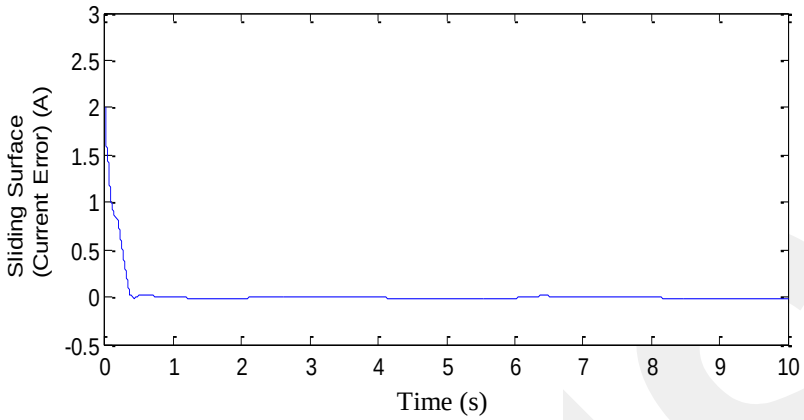

Figure 4.2.1.5 Current tracking error for PI-V plus PSMC.

4.2.2 Experimental Results

The experimental results of the cascade PI-V plus process SMC controller are illustrated in Figs. 4.2.2.1-5. Figure 4.2.2.1 shows that the controller holds the ball during startup and follows the reference position trajectory thereafter. The small oscillations around the reference point are due to the effects of sampling time, measurement error and noise. Furthermore, the ball sways right and left rather than staying vertically as the photo detector does not exactly measure the ball position because of circularly ball. This can be solved by touching lightly to the ball by hand. In 6^{th} second we touched the ball almost 0.5 second to center the ball, and after that point, it can be seen that the tracking results are improved.

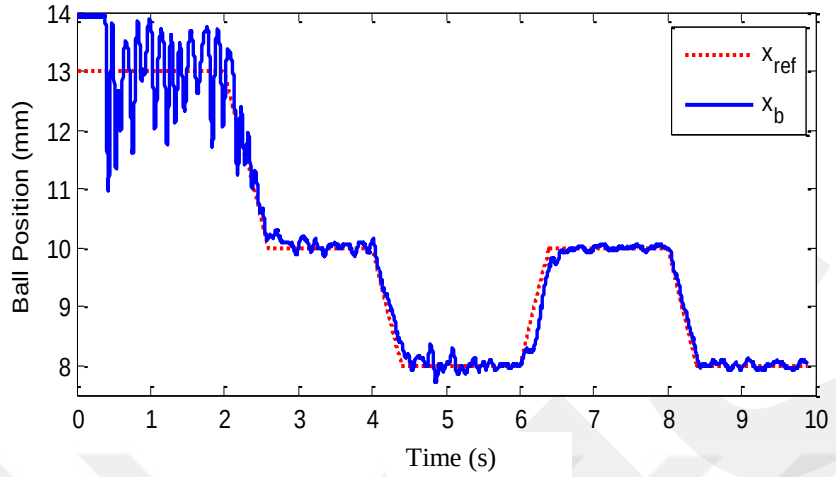

Figure 4.2.2.1 Experimental ball position trajectory for PI-V plus PSMC.

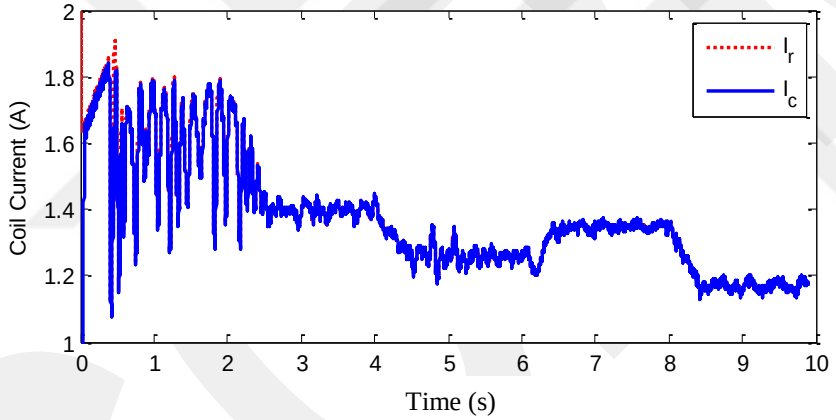

Figure 4.2.2.2 Experimental coil current response for PI-V plus PSMC.

Figure 4.2.2.2 shows the coil current response. Process SMC current controller eliminates the effects of inductance uncertainty and provides a highly satisfactory tracking performance. The response of the coil voltage is shown in Fig. 4.2.2.3. The average voltage supply is around 14V during steady-state. The position tracking error is shown in Fig. 4.2.2.4. The position error is clearly limited about 0.2mm during steady-state which satisfies desired requirements. The position error is decreased to 0.1mm after the light touch to the ball by hand. Figure 4.2.2.5 shows the sliding surface, *s*, (or current tracking error). It is seen that the sliding surface reaches zero in a short time and stays around zero thereafter.

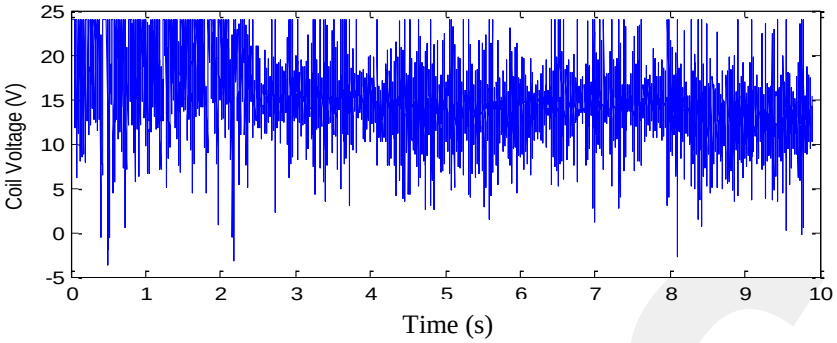

Figure 4.2.2.3 Experimental coil voltage response for PI-V plus PSMC.

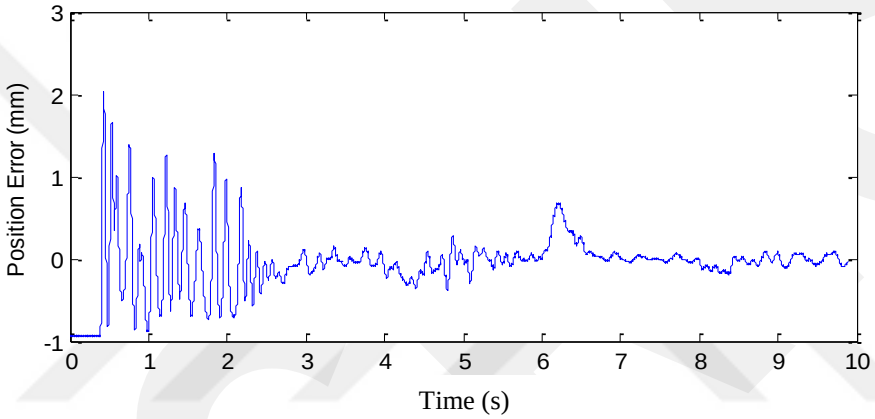

Figure 4.2.2.4 Experimental position tracking error for PI-V plus PSMC.

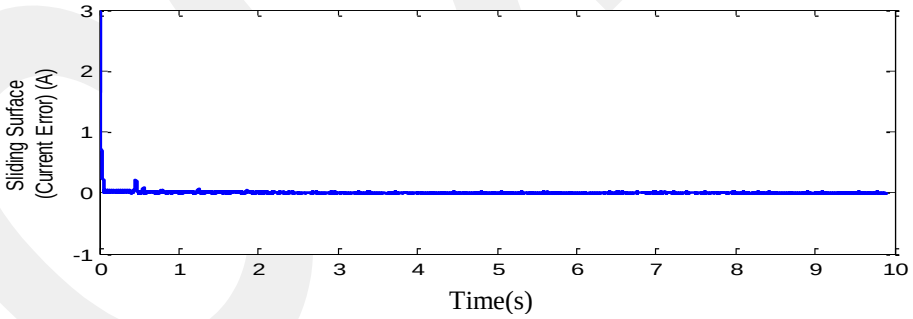

Figure 4.2.2.5 Experimental current tracking error for PI-V plus PSMC.

For the sinusoidal reference, the performance of the system under the proposed cascade control law is given in Figs. 4.2.2.6-10. The corresponding position tracking response is given in Fig. 4.2.2.6 where it is clear that the controller holds the ball during startup and follows the reference position trajectory thereafter. The coil current, coil voltage, position error and current error are given in Figs. 4.2.2.7-10, respectively. The reference tracking error

oscillates between ±0.1 mm as in pulse reference tracking case. It is also seen that the sliding surface (current error) reaches zero in a short time and stays around zero thereafter. We are able to achieve any kind of tracking with the process SMC based cascade control law.

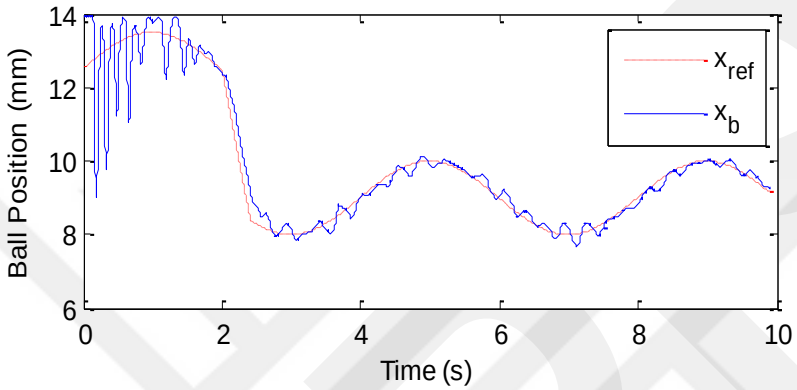

Figure 4.2.2.6 Experimental ball position trajectory for a sinusoidal reference of PI-V plus PSMC.

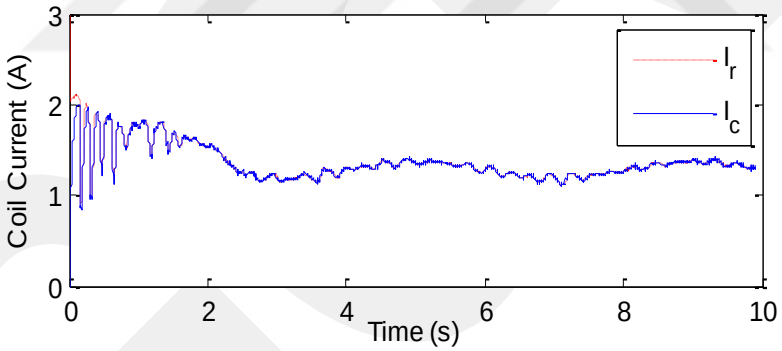

Figure 4.2.2.7 Experimental coil current response for a sinusoidal reference of PI-V plus PSMC.

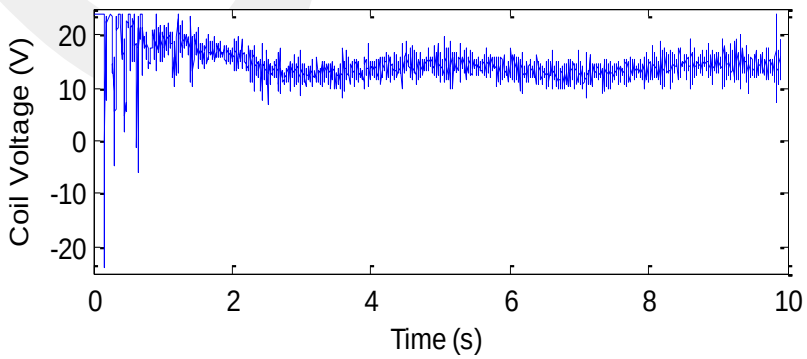

Figure 4.2.2.8 Experimental coil voltage response for a sinusoidal reference of PI-V plus PSMC.

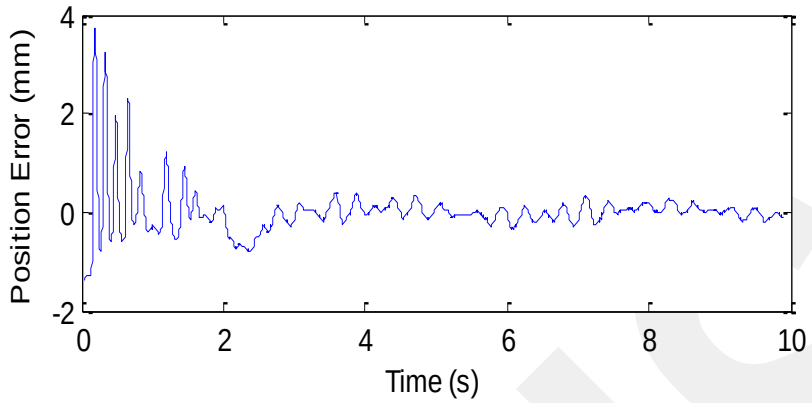

Figure 4.2.2.9 Experimental position tracking error for a sinusoidal reference of PI-V plus PSMC.

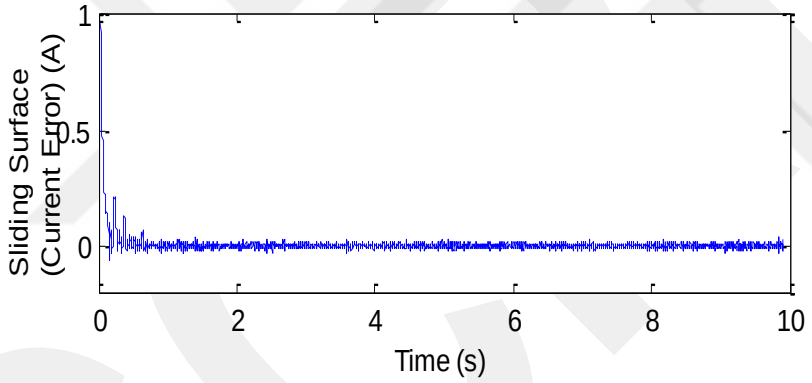

Figure 4.2.2.10 Experimental current tracking error for a sinusoidal reference of PI-V plus PSMC.

4.3 Integral SMC plus Process SMC Cascade Control

The integral SMC for the mechanical system and process SMC for the electrical part are appropriately cascaded. The experimental hardware-in-the-loop (HIL) test and numerical simulation results of this cascade control for the magnetic levitation are provided in this section.

4.3.1 Numerical Simulations

The tracking performances of the cascade integral SMC plus process SMC controller are shown in Figs. 4.3.1.1-5. It is seen in Fig. 4.3.1.1 that the controller provides a desired tracking performance with a little overshoot (almost 0.6%) and a little settling time (almost 0.26s. with 1% error). Thus, the ball position perfectly tracks the desired position. Figure 4.3.1.2 shows the response of the process SMC current controller in which the coil current perfectly tracks the desired current with around 0.008A error, which makes the ball to follow the reference trajectory. The tracking error, which is the difference between actual trajectory and reference trajectory, is shown in Fig. 4.3.1.3. The tracking error has little short transient response which satisfies the required settling time, and about 0.067mm (0.067% overshoot) in the simulations. Fig. 4.3.1.4 show that the sliding surface, *s*, (or current error) and, goes to zero in a short time and stays around zero for all subsequent times and 4.3.1.5 show that the sliding surface, s_1, for outer controller goes to zero in a short time and stays around zero with around 1% error for all subsequent times.

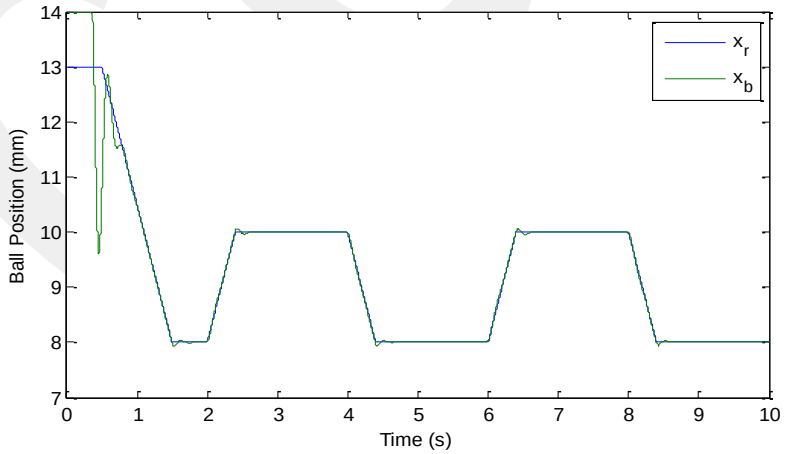

Figure 4.3.1.1 Ball position trajectory for ISMC plus PSMC.

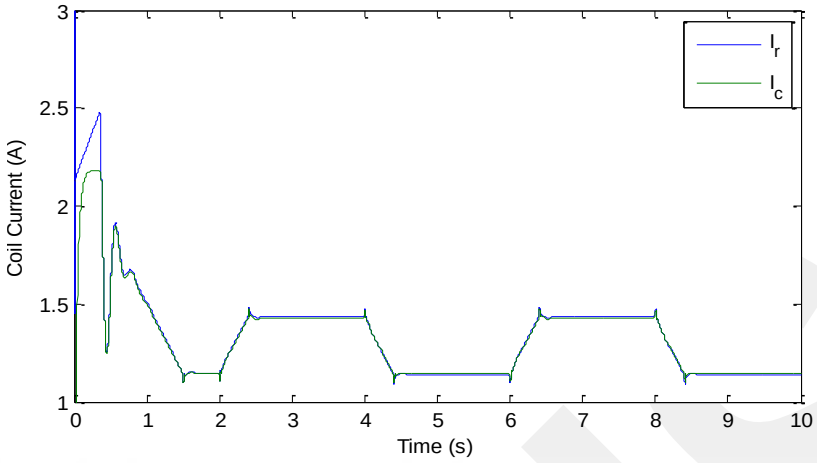

Figure 4.3.1.2 Coil current response for ISMC plus PSMC.

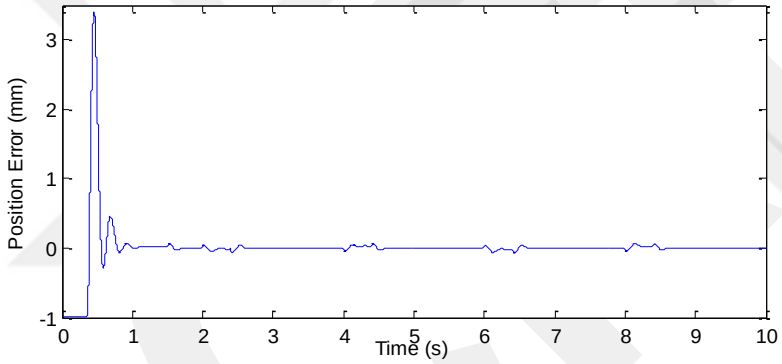

Figure 4.3.1.3 Position tracking error for ISMC plus PSMC.

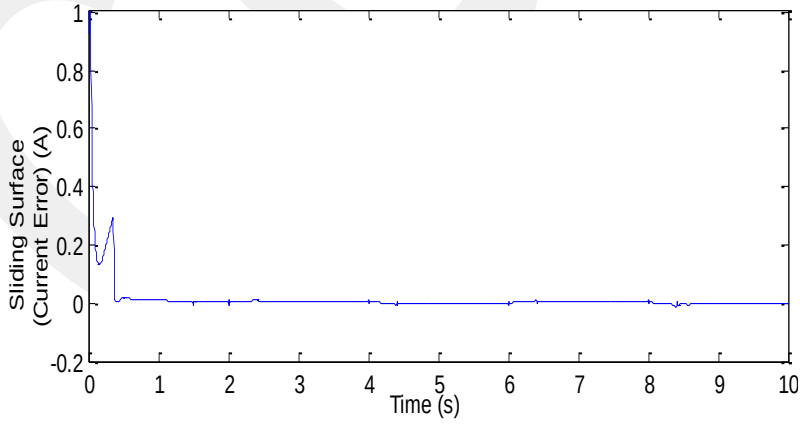

Figure 4.3.1.4 Current tracking error for ISMC plus PSMC.

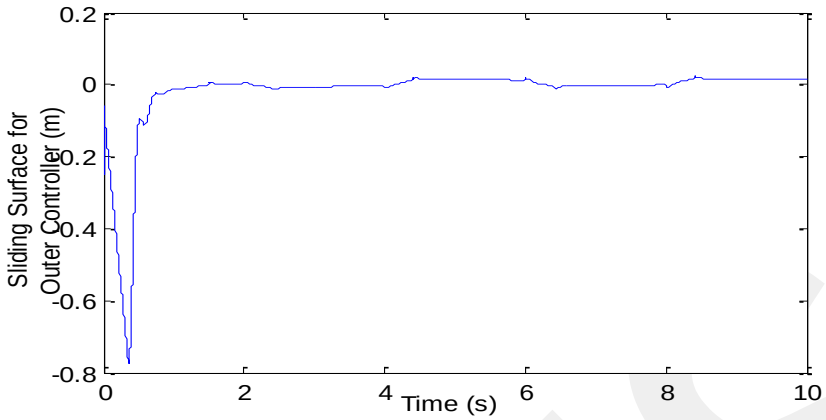

Figure 4.3.1.5 Sliding surface of outer ISMC for ISMC plus PSMC.

4.3.2 Experimental Results

The experimental results of the cascade integral SMC plus process SMC controller are shown in Figures 4.3.2.1-7. Figure 4.3.2.1 shows that the controller holds the ball during startup and follows the reference position trajectory thereafter with around 1.5% error. The small oscillations around the reference point are due to the effects of sampling time, measurement error and noise. In addition, the ball sways right and left rather than staying vertically as the photo detector does not exactly measure the ball position because of the circularity of the ball. This can be solved with touching lightly to the ball by hand.

Figure 4.3.2.2 shows the response of the coil current. The process SMC current controller eliminates the effects of inductance uncertainty and provides a highly satisfactory tracking performance. The position tracking error around 1.5% is shown in Figure 4.3.2.3. Figure 4.3.2.4 shows the sliding surface, *s*, (or current tracking error). It is seen that the sliding surface reaches zero in a short time and stays around zero with average 0.01A error thereafter. Figure 4.3.2.5 shows the sliding surface, s_1, for the ball position controller. It is seen that the sliding surface reaches zero in a short time and stays around zero with average 0.2% error thereafter.

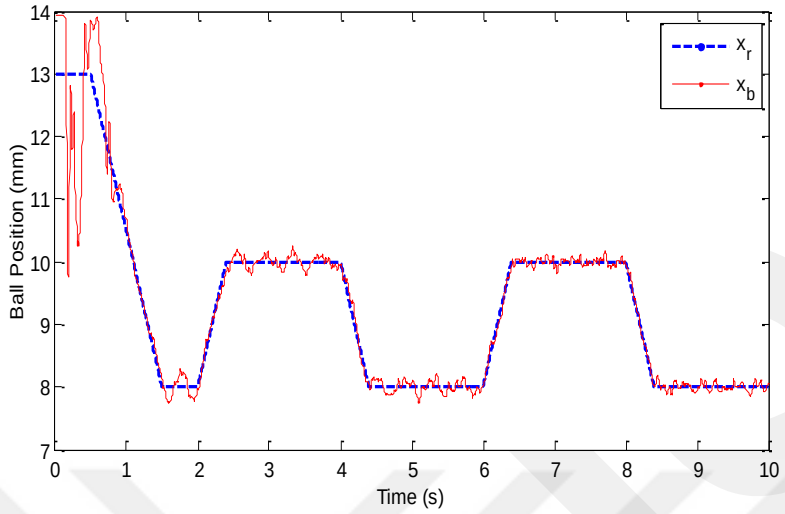

Figure 4.3.2.1 Experimental ball position trajectory for ISMC plus PSMC.

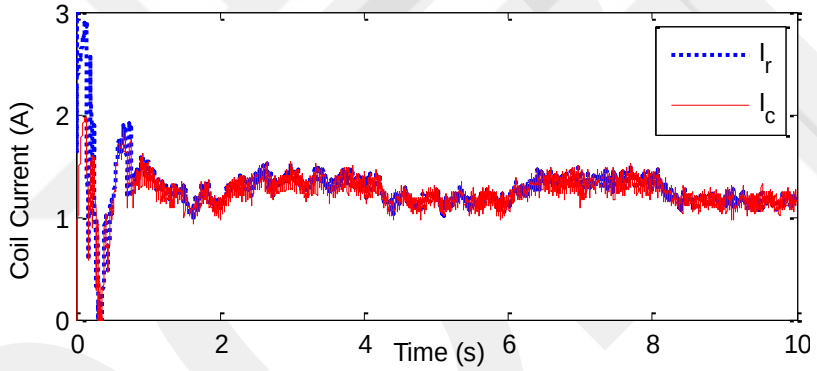

Figure 4.3.2.2 Experimental coil current response for ISMC plus PSMC.

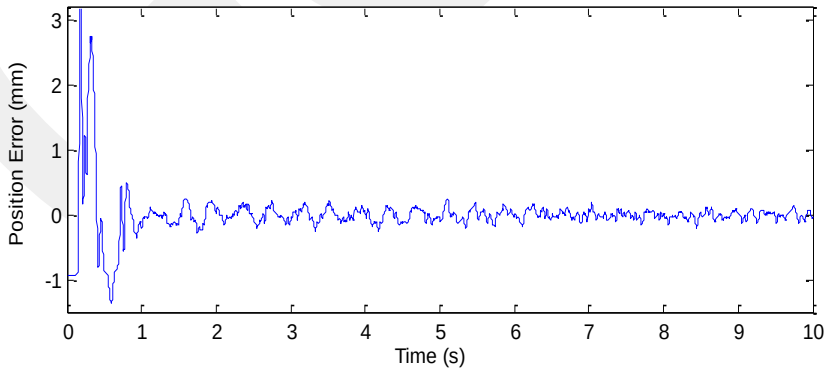

Figure 4.3.2.3 Experimental position tracking error for ISMC plus PSMC.

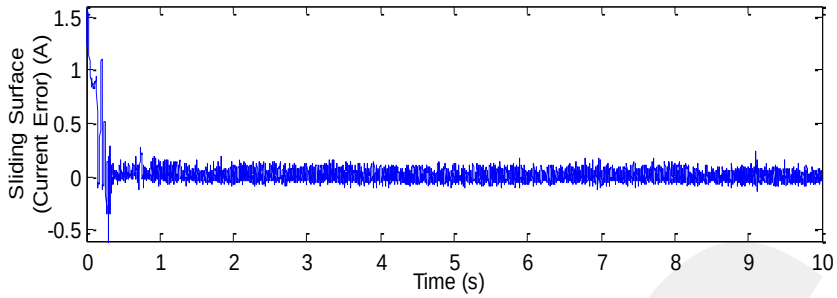

Figure 4.3.2.4 Experimental current tracking error for ISMC plus PSMC.

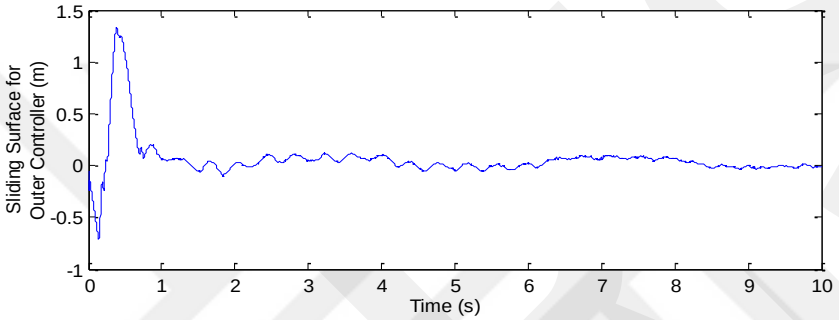

Figure 4.3.2.5 Experimental sliding surface of outer ISMC for ISMC plus PSMC.

Moreover, it can be said that the ball position trajectory error decreases due to the progressive simulation. In Figures 4.3.2.6-7, the steady-state behavior of the system is illustrated from 40 to 50 seconds. In Figure 4.3.2.7, the position clearly error is limited about 0.1mm during steady-state which satisfies desired requirements.

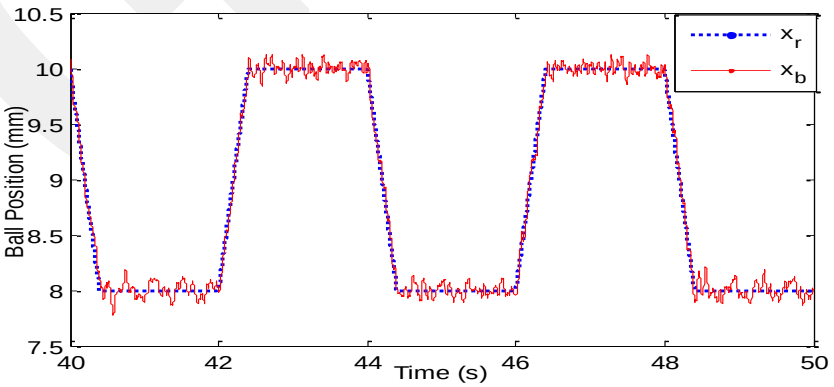

Figure 4.3.2.6 Experimental ball position trajectory in the steady-state for ISMC plus PSMC.

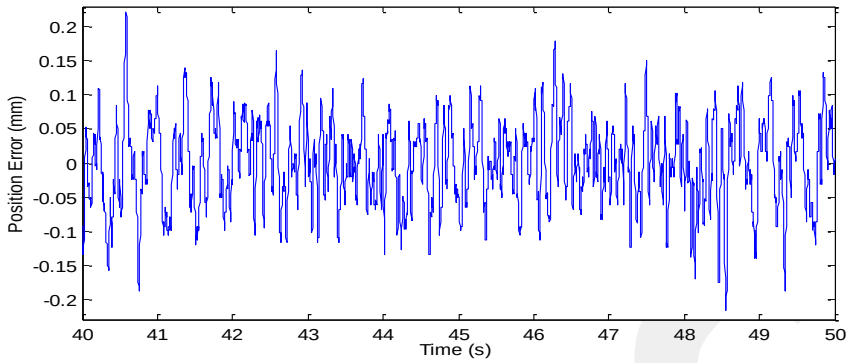

Figure 4.3.2.7 Experimental position tracking error in the steady-state for ISMC plus PSMC.

4.4 Integral SMC plus Equivalent SMC Cascade Control with Varying Inductance

The integral SMC for the mechanical system and equivalent SMC with the coil inductance dependent on the ball position for the electrical part are cascaded properly. The experimental hardware-in-the-loop (HIL) test and numerical simulation results of this cascade control for the magnetic levitation are provided in this section.

4.4.1 Numerical Simulations

The numerical simulation results of the cascade integral SMC plus equivalent SMC controller is illustrated in Figs. 4.4.1.1-5. It is shown in Fig. 4.4.1.1 that the controller provides a desired tracking performance with a little overshoot (around 0.5%). Figure 4.4.1.2 shows the response of the equivalent SMC current controller in which the coil current perfectly tracks the desired current, which makes the ball to follow the reference trajectory. The tracking error, which is the difference between actual trajectory and reference trajectory, is shown in Fig. 4.4.1.3. The tracking error has little short transient response

which satisfies the required settling time, and about 0.05mm (0.5% overshoot) in the simulations. Fig. 4.4.1.4 show that the sliding surface, *s*, (or current error) and, goes to zero in a short time and stays around zero for all subsequent times and 4.4.1.5 show that the sliding surface, s_1, for outer controller goes to zero in a short time and stays around zero with around 0.01% error for all subsequent times.

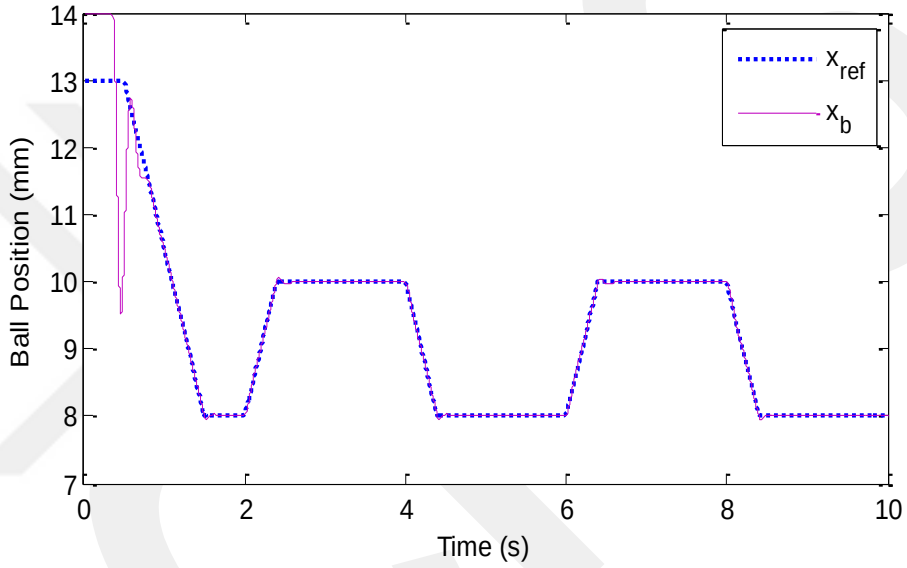

Figure 4.4.1.1 Ball position trajectory for ISMC plus eSMC with varying inductance.

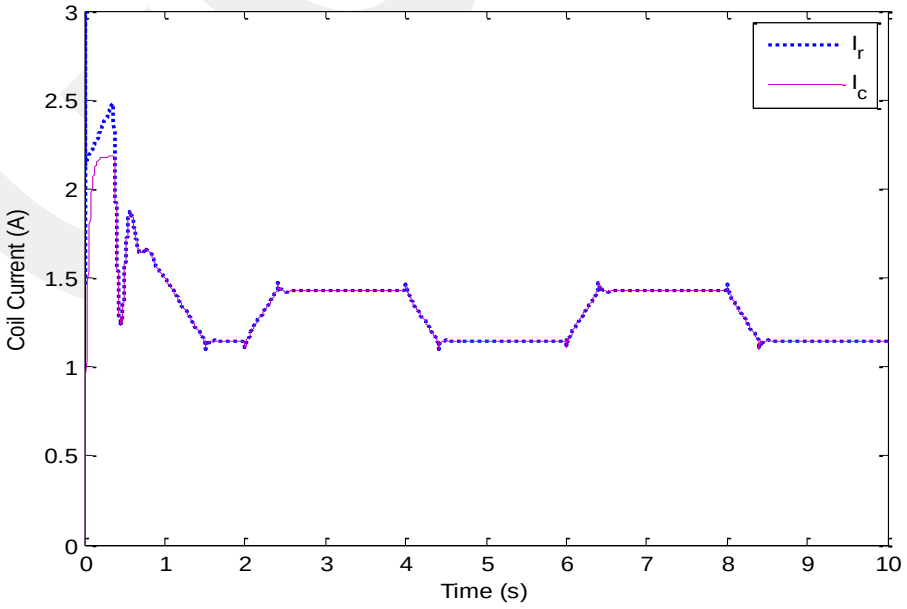

Figure 4.4.1.2 Coil current response for ISMC plus eSMC with varying inductance.

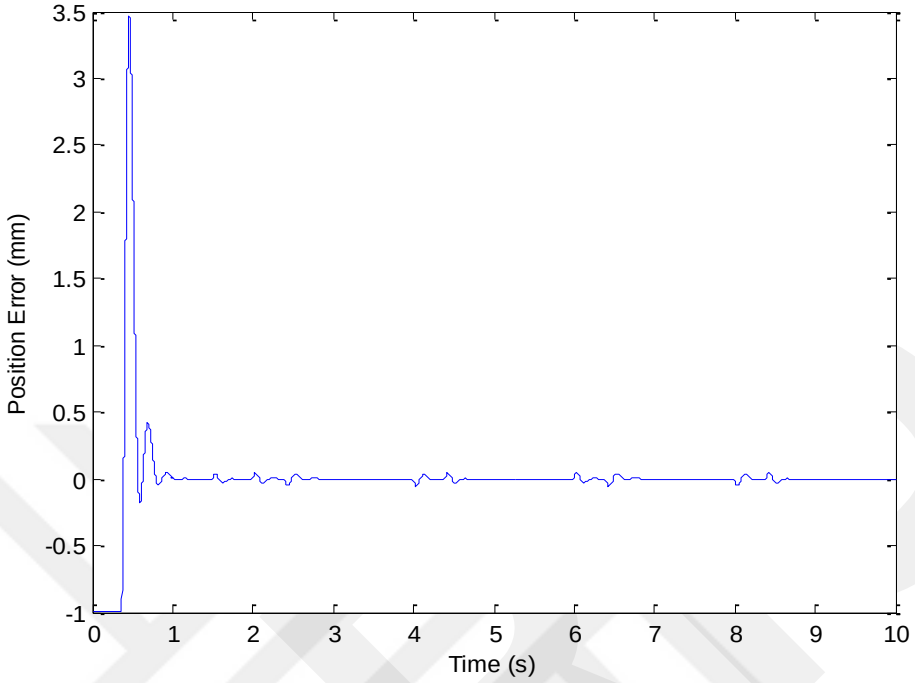

Figure 4.4.1.3 Ball position tracking error for ISMC plus eSMC with varying inductance.

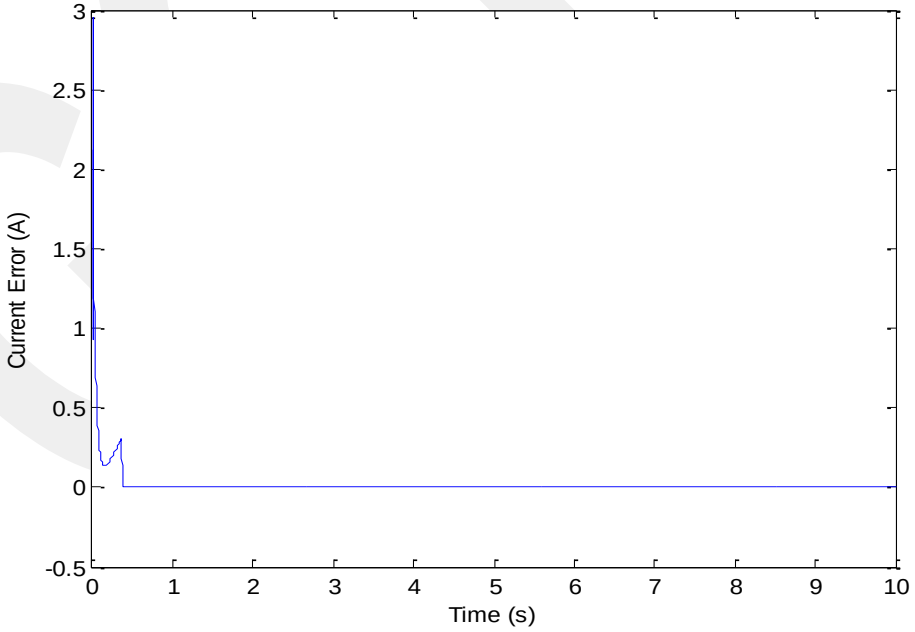

Figure 4.4.1.4 Current tracking error for ISMC plus eSMC with varying inductance.

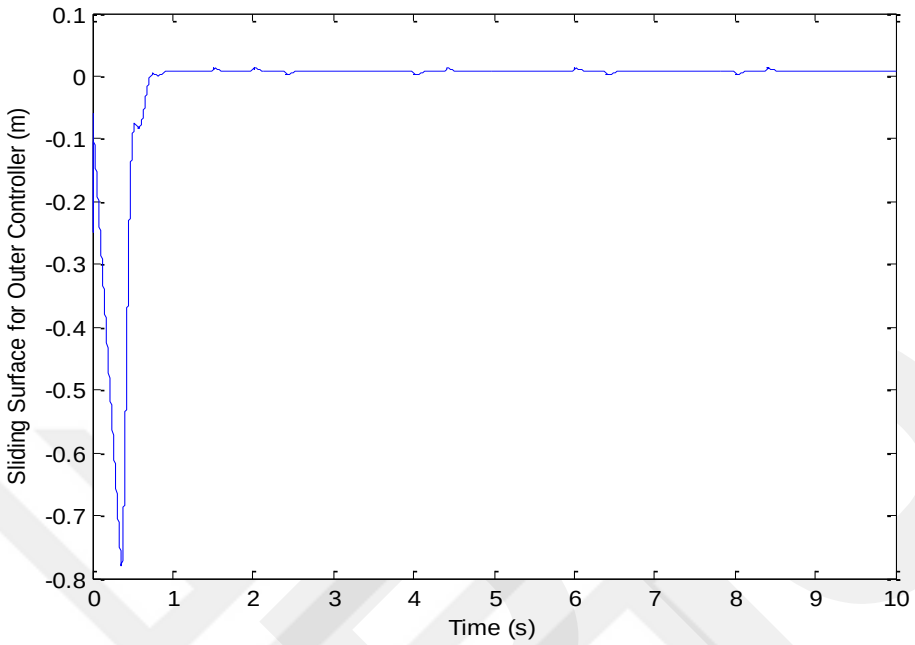

Figure 4.4.1.5 Sliding surface of outer ISMC for ISMC plus eSMC with varying inductance.

4.4.2 Experimental Results

The experimental results of the cascade integral SMC plus equivalent SMC controller with varying inductance are shown in Figures 4.4.2.1-5. Figure 4.4.2.1 shows that the controller holds the ball during startup and follows the reference position trajectory thereafter with around 0.07mm error (0.7% overshoot). The small oscillations around the reference point are due to the effects of sampling time, measurement error and noise. In addition, the ball sways right and left rather than staying vertically as the photo detector does not exactly measure the ball position because of the circularity of the ball. This can be solved by touching lightly to the ball by hand.

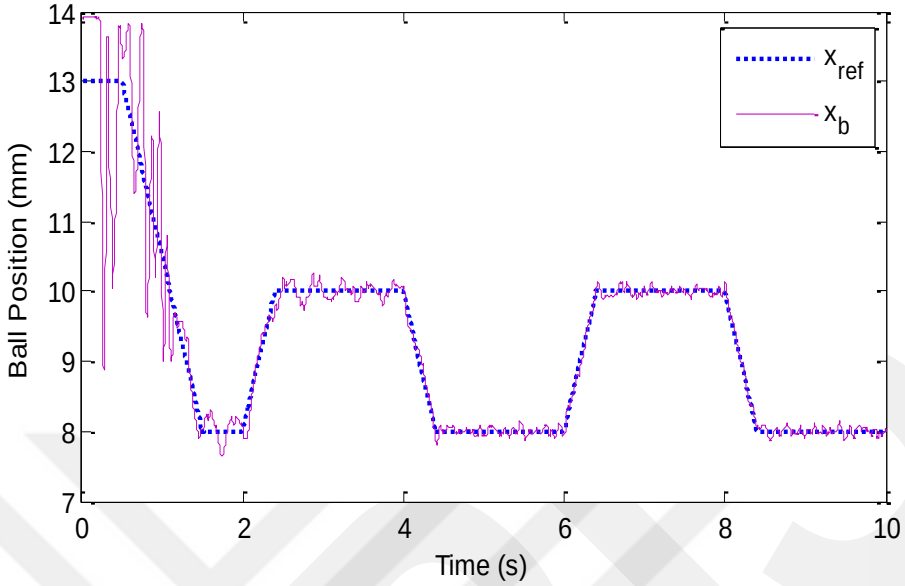

Figure 4.4.2.1 Experimental ball position trajectory for ISMC plus eSMC with varying inductance.

Figure 4.4.2.2 shows the response of the coil current. The equivalent SMC current controller eliminates the effects of inductance uncertainty and provides a highly satisfactory tracking performance. The position tracking error around 0.7% (0.07mm) in steady-state is shown in Figure 4.4.2.3. Figure 4.4.2.4 shows the sliding surface, *s*, (or current tracking error). It is seen that the sliding surface reaches zero in a short time and stays around zero. Figure 4.4.2.5 shows the sliding surface, s_1, for the ball position controller. It is seen that the sliding surface reaches zero in a short time and stays around zero with average 0.5% error thereafter.

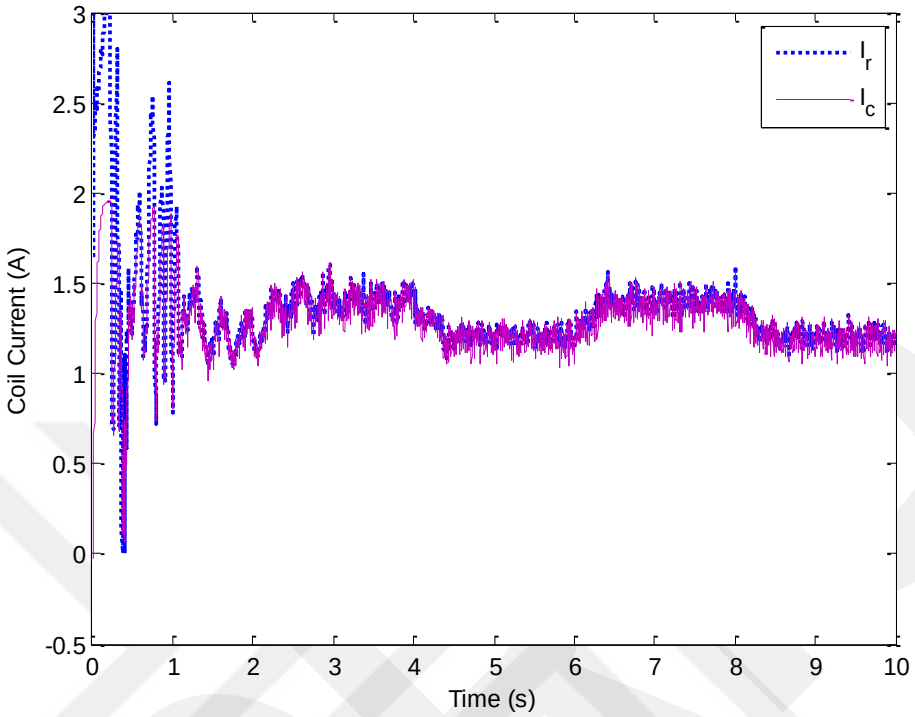

Figure 4.4.2.2 Experimental coil current response for ISMC plus eSMC with varying inductance.

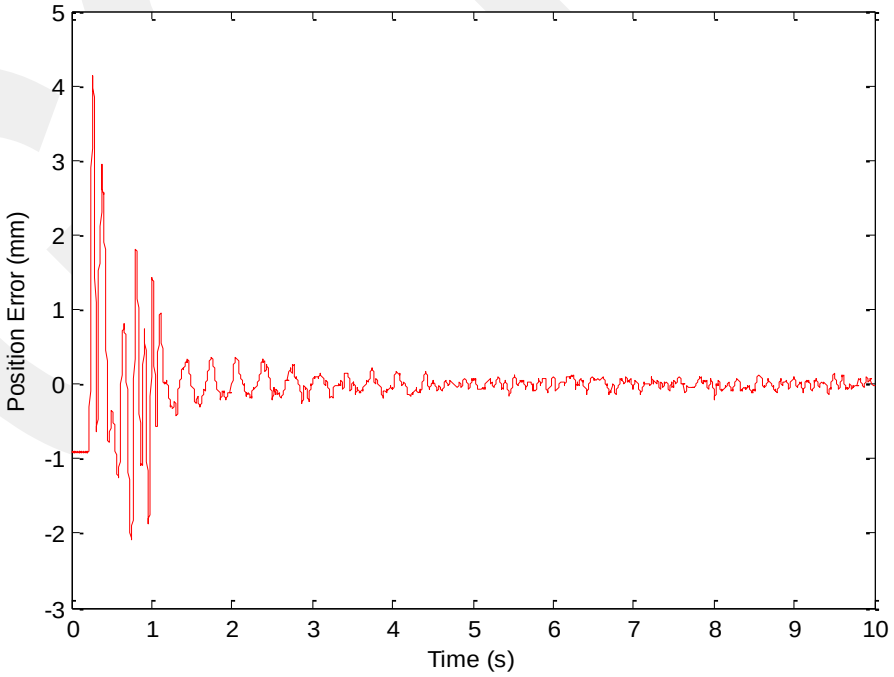

Figure 4.4.2.3 Experimental position tracking error for ISMC plus eSMC with varying inductance.

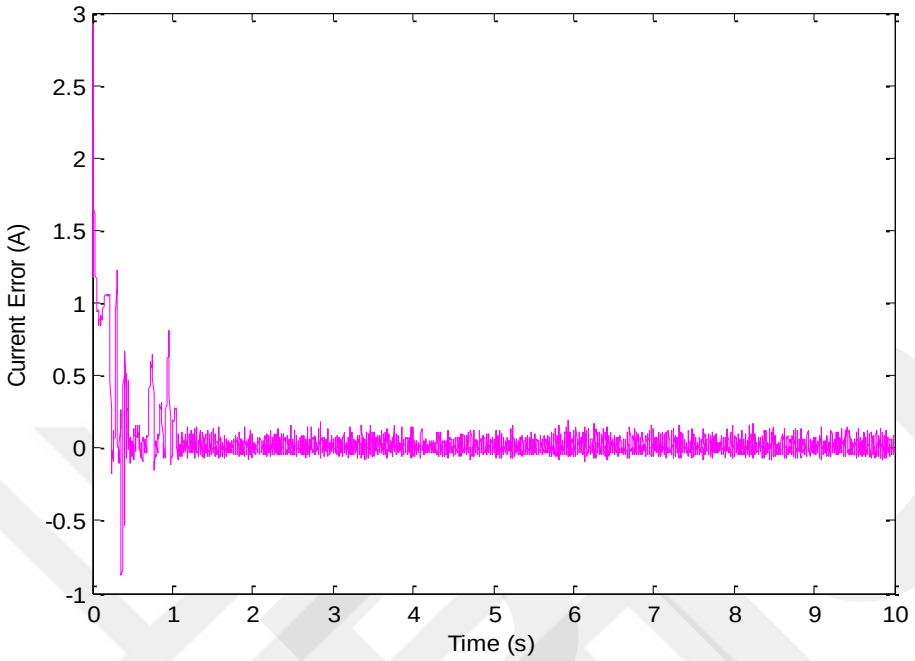

Figure 4.4.2.4 Experimental current tracking error for ISMC plus eSMC with varying inductance.

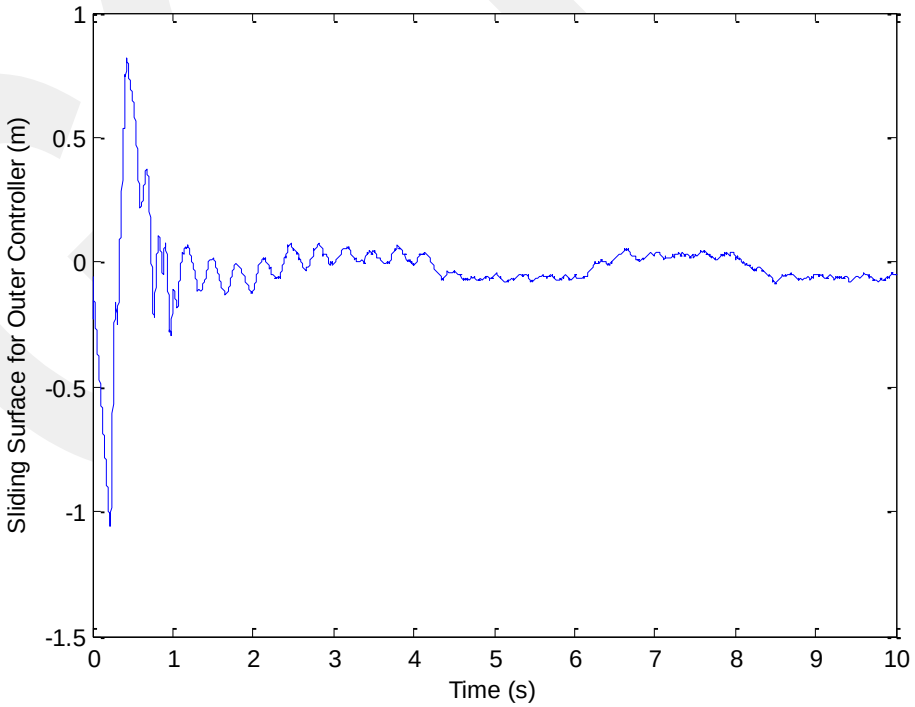

Figure 4.4.2.5 Experimental sliding surface of outer ISMC for ISMC plus eSMC with varying inductance.

4.5 Comparison of Cascade Controllers

4.5.1 Numerical Simulations

According to the percent overshoot, settling time with 2% error, the position error, the current error and the sliding surface (s_1) of sliding mode based controllers designed for the mechanical part as the outer controller, comparisons of numerical simulation results of all cascade controllers are shown in Table 4.5.1.1. Here, PI-V controller for the outer loop does not have sliding surface of the outer controller. Numerical simulation clearly presents the differences between controllers. According to Table 4.5.1.1, when PI-V is designed as an outer controller, the results of the ball position tracking performance are almost same with little errors. The position error is almost 0.22mm and the settling time is 0.3 second 2% with error. Moreover, when the traditional sliding mode controller is designed as an outer controller, the results are almost same as a percent overshoot or a position error, but settling time is 0.5 second with 6% error and does not achieve the desired performance requirement (the maximum settling time ≤ 0.3s.). On the other hand, when the integral sliding mode controller is designed as an outer controller, the position error is almost 0.6mm and settling time is 0.19 second with 2% error or 0.26 second with 1% error. Therefore, the cascade controllers provide wonderful performances for the ball position of the magnetic levitation system in the numerical simulations.

Controller	Percent Overshoot (PO)	Settling Time (s)	Position Error (mm)	Current Error(s) (A)	Sliding Surface(s_1) (m)
PI-V plus PI	2.3%	0.3	0.22	0.0005	-
PI-V plus high-gain SMC	2.3%	0.3	0.22	0.006	-
PI-V plus PSMC	2.2%	0.3	0.22	0.005	-
PI-V plus eSMC with varying inductance	2.2%	0.3	0.21	0.00002	-
PI-V plus PSMC with varying inductance	2.2%	0.3	0.21	0.004	-
SMC plus high-gain SMC	2%	0.5	0.13	0.03	0.01
ISMC plus high-gain SMC	0.6%	0.19	0.06	0.008	0.012
ISMC plus PSMC	0.6%	0.19	0.06	0.008	0.015
ISMC plus eSMC with varying inductance	0.5%	0.19	0.05	0.0007	0.01
ISMC plus PSMC with varying inductance	0.55%	0.19	0.05	0.007	0.012

Table 4.5.1.1 Position tracking performance of numerical studies for all cascaded controllers.

4.5.2 Experimental Results

In experimental studies, the small oscillations around the reference point are due to the effects of sampling time, measurement error and noise. In addition, the ball sways right and left rather than staying vertically as the photo detector does not exactly measure the ball position because of the circularity of the ball. This can be solved with touching lightly to the ball by hand.

For experimental studies, the comparisons of the ball position tracking performance of all cascade controllers are shown in Table 4.5.2.1. The performance comparisons are done according to the percent overshoot, the position error, the current error and the sliding surface (s_1) of sliding mode based controllers designed for the mechanical part as the outer controller, Here, PI-V controller for the outer loop does not have sliding surface. The settling time may not be measured for the experimental results due to the oscillations. According to Table 4.5.2.1, when PI-V is designed as an outer controller, the results of the ball position tracking performance are almost same with little error. Moreover, when the traditional sliding mode controller is designed as an outer controller, the controller does not satisfy the desired settling time and it has a large maximum percent overshoot. On the other hand, when the integral sliding mode controller is designed as an outer controller, the cascade controllers provide wonderful performance for the ball position of the magnetic levitation system in the experimental results. ISMC plus eSMC with varying inductance cascade controller provides the best performance for the tracking ball position for the magnetic levitation system.

Controller	Percent Overshoot (PO)	Settling Time (s)	Position Error (mm)	Current Error(s) (A)	Sliding Surface (s_1) (m)
PI-V plus PI	2.3%	-	0.23	0.03	-
PI-V plus high-gain SMC	2%	-	0.2	0.03	-
PI-V plus PSMC	2%	-	0.2	0.02	-
PI-V plus eSMC with varying inductance	2.1%	-	0.2	0.01	-
PI-V plus PSMC with varying inductance	2%	-	0.2	0.02	-
SMC plus high-gain SMC	6.5%	-	0.6	0.03	0.05
ISMC plus high-gain SMC	1.8%	-	0.18	0.02	0.05
ISMC plus PSMC	1.5%	-	0.15	0.01	0.05
ISMC plus eSMC with varying inductance	1%	-	0.07	0.02	0.05
ISMC plus PSMC with varying inductance	1%	-	0.08	0.03	0.05

Table 4.5.2.1 Position tracking performance of experimental studies for all cascaded controllers.

Chapter 5

Conclusions

Magnetic levitation systems are used to provide frictionless movement, reliable and economical operations in many industrial applications. On the other hand, the magnetic levitation system is a highly nonlinear system, and has the electromagnet inductance originated parameter uncertainty and open-loop unstable dynamics. All these challenges need the design of precise feedback control systems. To deal with the issues of the magnetic levitation technology, sliding mode control which is a robust nonlinear control method is designed to provide a stable and robust magnetic levitation operations.

A cascade controller with sliding mode and PID controllers is designed for feedback control of the magnetic levitation to increase the position tracking performance in this thesis. The cascade controller consists of an inner current loop and an outer position loop. For the inner loop, SMC based cascade controllers are designed to eliminate the coil parameter uncertainty and to give fast response. For the outer position loop, both SMC and PIV based controllers are designed to decrease the effects of disturbances around the operating point. The nonlinear system model and its linearization are taken into account in the control designs. Both numerical simulation and experimental results are provided and it is shown that the SMC based cascade controller provides a highly precise position tracking performance. The SMC controllers keeps the current error around zero and provides ±0.1 mm position error in the steady-state, which is very small compared to the literature.

BIBLIOGRAPHY

[1] Y. Luguang, "Progress of the Maglev Transportation in China," *IEEE Transactions on Applied Superconductivity*, vol. 16, no. 2, pp. 1138–1141, Jun. 2006.

[2] D. F. Berdy, D. J. Valentino, and D. Peroulis, "Kinetic energy harvesting from human walking and running using a magnetic levitation energy harvester," *Sensors and Actuators A: Physical*, vol. 222, pp. 262–271, Feb. 2015.

[3] K. Ozturk, E. Sahin, M. Abdioglu, M. Kabaer, S. Celik, E. Yanmaz, and T. Kucukomeroglu, "Comparative study of the magnetic stiffness, levitation and guidance force properties of single and multi seeded YBCOs for different HTS–PMG arrangements," *Journal of Alloys and Compounds*, vol. 643, pp. 201–206, Sep. 2015.

[4] A. El Hajjaji and M. Ouladsine, "Modeling and nonlinear control of magnetic levitation systems," *IEEE Transactions on Industrial Electronics*, vol. 48, no. 4, pp. 831–838, Aug. 2001.

[5] U. Hasirci, A. Balikci, Z. Zabar, and L. Birenbaum, "A Novel Magnetic-Levitation System: Design, Implementation, and Nonlinear Control," *IEEE Transactions on Plasma Science*, vol. 39, no. 1, pp. 492–497, Jan. 2011.

[6] W. Barie and J. Chiasson, "Linear and nonlinear state-space controllers for magnetic levitation," *International Journal of Systems Science*, vol. 27, no. 11, pp. 1153–1163, Nov. 1996.

[7] S. Yamamura and H. Yamaguchi, "Electromagnetic levitation system by means of salient-pole type magnets coupled with laminated slotless rails," *IEEE Transactions on Vehicular Technology*, vol. 39, no. 1, pp. 83–87, 1990.

[8] D. Cho, Y. Kato, and D. Spilman, "Sliding mode and classical controllers in magnetic levitation systems," *IEEE Control Systems*, vol. 13, no. 1, pp. 42–48, Feb. 1993.

[9] F. Beltran-Carbajal, A. Valderrabano-Gonzalez, J. C. Rosas-Caro, and A. Favela-Contreras, "Output feedback control of a mechanical system using magnetic levitation," *ISA Transactions*, vol. 57, pp. 352–359, Jul. 2015.

[10] R. Morales and H. Sira-Ramírez, "Trajectory tracking for the magnetic ball levitation system via exact feedforward linearisation and GPI control," *International Journal of Control*, vol. 83, no. 6, pp. 1155–1166, Jun. 2010.

[11] C. Nielsen, C. Fulford, and M. Maggiore, "Path following using transverse feedback linearization: Application to a maglev positioning system," in *American Control Conference, 2009. ACC '09.*, 2009, pp. 3045–3050.

[12] O. M. El Rifai and K. Youcef-Toumi, "Achievable performance and design trade-offs in magnetic levitation control," in *, 1998 5th International Workshop on Advanced Motion Control, 1998. AMC '98-Coimbra*, 1998, pp. 586–591.

[13] Y. C. Kim and K.-H. Kim, "Gain scheduled control of magnetic suspension system," in *American Control Conference, 1994*, 1994, vol. 3, pp. 3127–3131 vol.3.

[14] S.-Y. Chen, F.-J. Lin, and K.-K. Shyu, "Direct decentralized neural control for nonlinear MIMO magnetic levitation system," *Neurocomputing*, vol. 72, no. 13–15, pp. 3220–3230, Aug. 2009.

[15] N. F. Al-Muthairi and M. Zribi, "Sliding mode control of a magnetic levitation system," *Mathematical Problems in Engineering*, vol. 2004, no. 2, pp. 93–107, 2004.

[16] F.-J. Lin, S.-Y. Chen, and K.-K. Shyu, "Robust Dynamic Sliding-Mode Control Using Adaptive RENN for Magnetic Levitation System," *IEEE Transactions on Neural Networks*, vol. 20, no. 6, pp. 938–951, Jun. 2009.

[17] F.-J. Lin, L.-T. Teng, and P.-H. Shieh, "Intelligent Adaptive Backstepping Control System for Magnetic Levitation Apparatus," *IEEE Transactions on Magnetics*, vol. 43, no. 5, pp. 2009–2018, May 2007.

[18] T. Bächle, S. Hentzelt, and K. Graichen, "Nonlinear model predictive control of a magnetic levitation system," *Control Engineering Practice*, vol. 21, no. 9, pp. 1250–1258, Sep. 2013.

[19] E. V. Kumar and J. Jerome, "LQR based Optimal Tuning of PID Controller for Trajectory Tracking of Magnetic Levitation System," *Procedia Engineering*, vol. 64, pp. 254–264, 2013.

[20] Hassan K. Khalil, "Nonlinear Control," Prentice Hall, first edition (2014).

[21] V. Utkin, J. Guldner and J. Shi, "Sliding Mode Control in Electro-Mechanical Systems," CRC Press, second edition (2009).

[22] J. Baranowski and P. Piatek, "Observer-based feedback controller for the magnetic levitation system," Transactions of the Institute of Measurement and Control, vol. 34, no.1, pp. 422-435, Mar. 2012.

[23] B. V. Jayawant and D. P. Rea, "New electromagnetic suspension and its stabilisation," *Proceedings of the Institution of Electrical Engineers*, vol. 115, no. 4, pp. 549–554, Apr. 1968.

[24] G. Ablay, "Variable structure controllers for unstable processes," *Journal of Process Control*, vol. 32, pp. 10–15, Aug. 2015.

[25] G. Ablay and Y. Eroglu, "Variable structure controllers for processes," in *Turkish Automatic Control Conference, TOK2015*, Denizli, 2015.

APPENDIX

Appendix A: Simulink Programs

The following Simulink programs are used in the numerical and experimental studies.

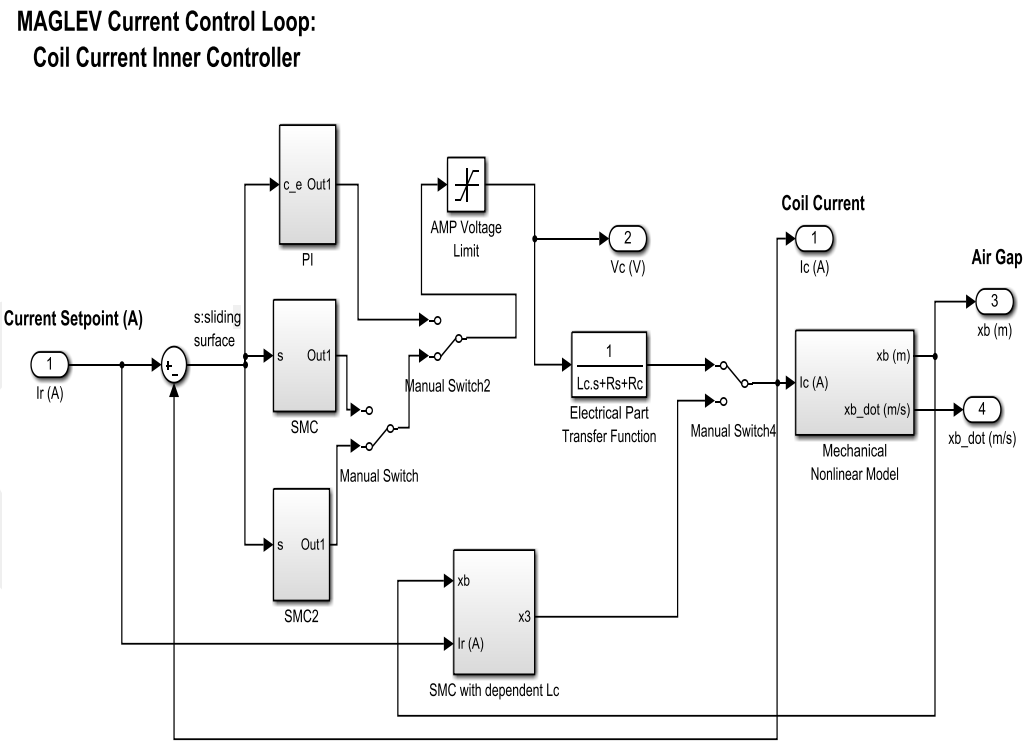

Figure A.1 Block diagram of the inner current control with PI, high-gain SMC, PSMC and SMC with varying inductance.

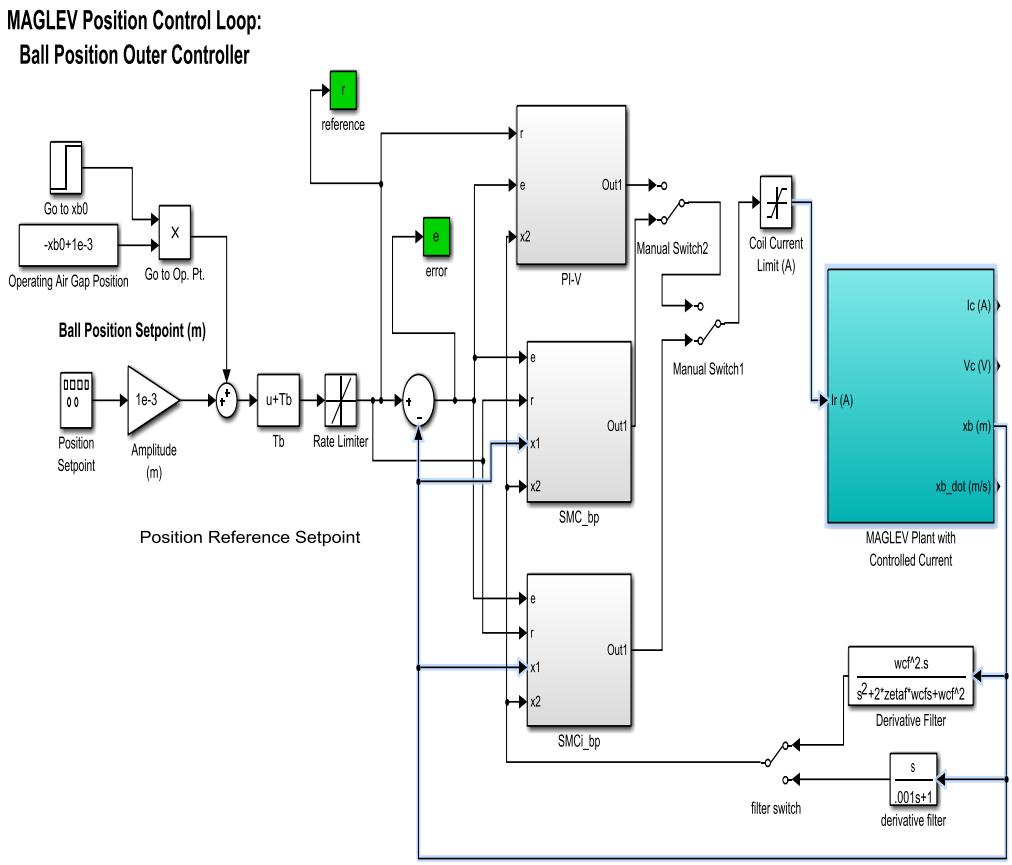

Figure A.2 Block diagram of the outer ball position control with PI-V controller, SMC and integral SMC.

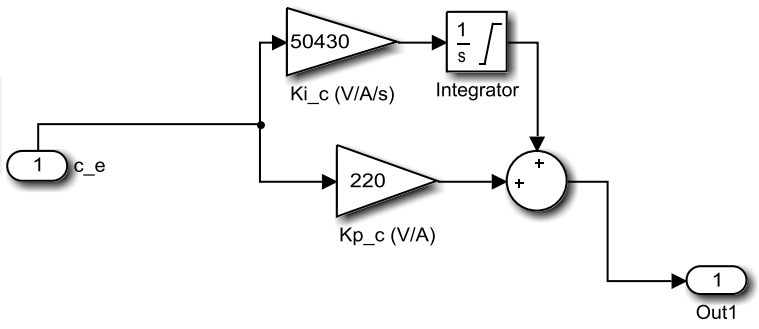

Figure A.3 Block diagram of the PI controller.

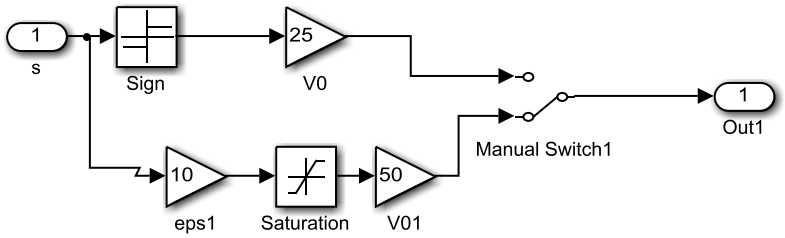

Figure A.4 Block diagram of the high-gain SMC.

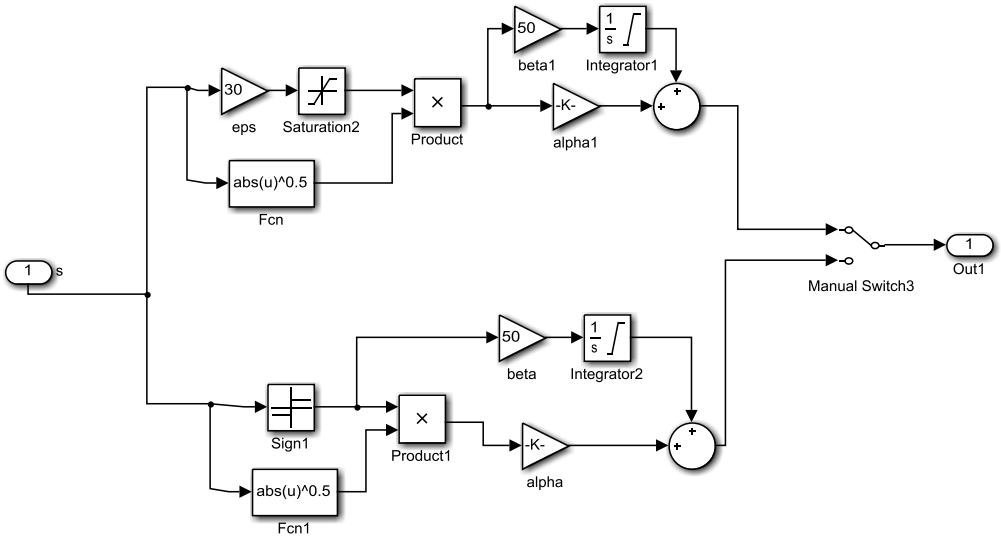

Figure A.5 Block diagram of the process SMC.

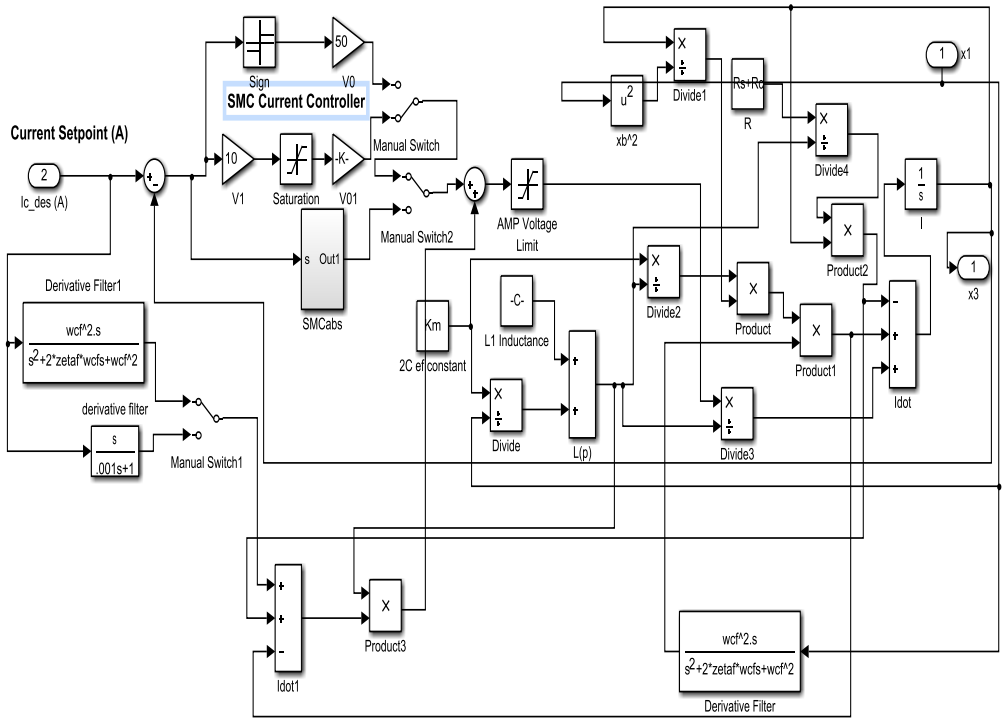

Figure A.6 Block diagram of the SMC with varying inductance.

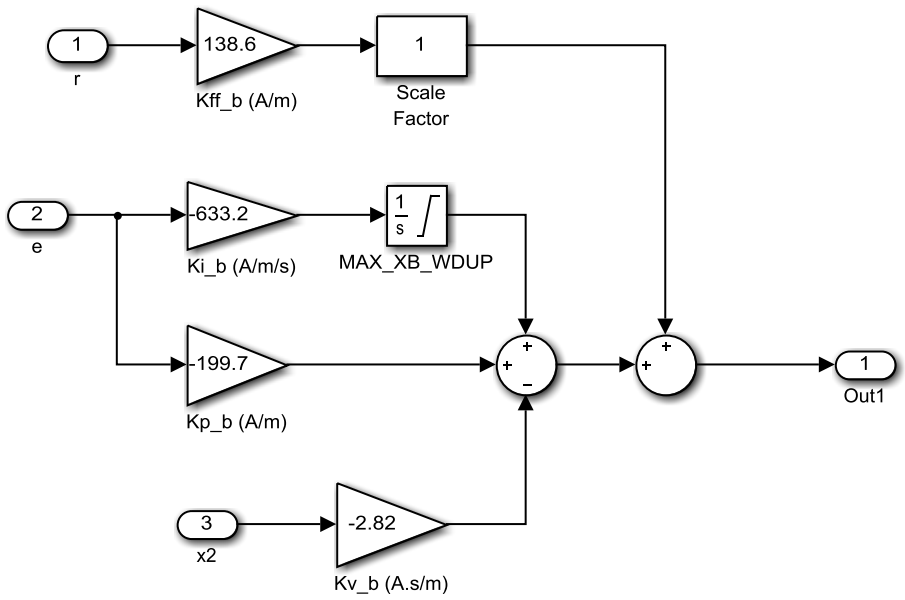

Figure A.7 Block diagram of the PI-V controller.

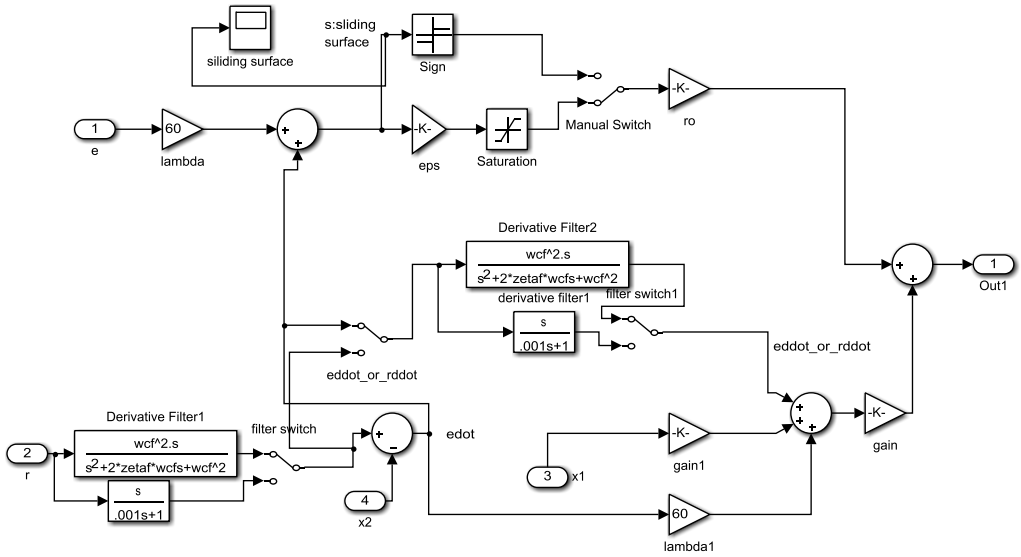

Figure A.8 Block diagram of the SMC controller.

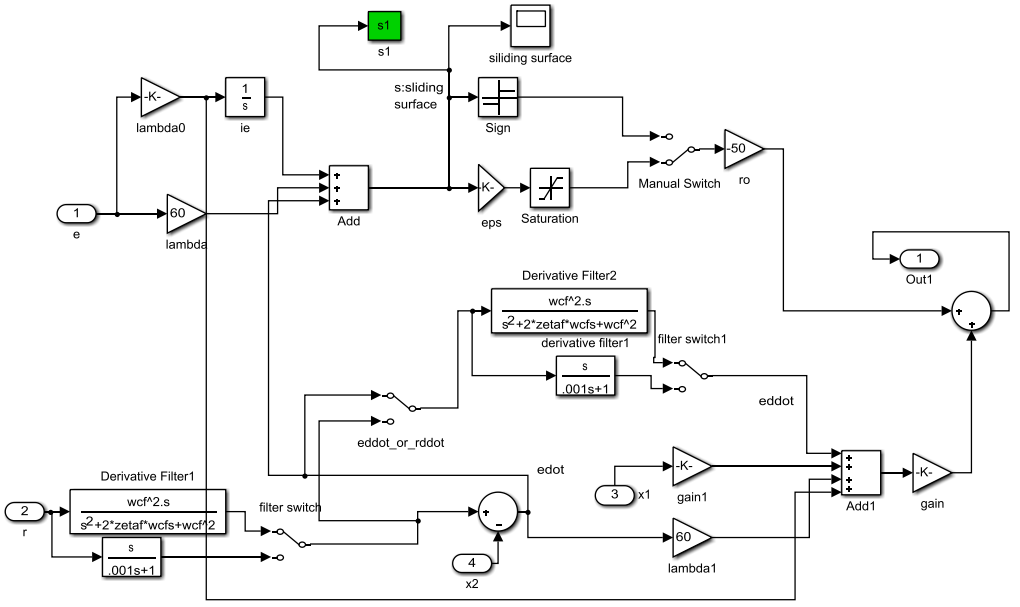

Figure A.9 Block diagram of the integral SMC controller.

Appendix B: Taylor Series Approximation

The Taylor series approximation is used to linearize the nonlinear systems and, for a nonlinear function $f(z)$, described by

$$f(z) = f(z_0) + \left.\left(\frac{\partial f(z)}{\partial z}\right)\right|_{z=z_0} (z - z_0) + \left.\left(\frac{\partial^2 f(z)}{\partial z^2}\right)\right|_{z=z_0} (z - z_0)^2 + \ldots \quad \textbf{(B1)}$$

where z_0 is the operating point.